Ocean Engineering 244 (2022) 110378

Contents lists available at ScienceDirect

Ocean Engineering

journal homepage: www.elsevier.com/locate/oceaneng

Numerical studies on CALM buoy motion responses and the effect of buoy geometry cum skirt dimensions with its hydrodynamic waves-current interactions

Chiemela Victor Amaechi [a,b,*], Facheng Wang [c], Jianqiao Ye [a,**]

[a] Engineering Department, Lancaster University, Lancaster, LA1 4YR, UK
[b] Standard Organisation of Nigeria (SON), 52 Lome Crescent, Wuse Zone 7, Abuja, 900287, Nigeria
[c] Department of Civil Engineering, Tsinghua University, Beijing, 100084, China

ARTICLE INFO

Keywords:
Ocean hydrodynamics
Waves-current interaction (WCI)
CALM Buoy skirt
Floating offshore structure (FOS)
Response amplitude operator (RAO)
Hydrodynamic motion response

ABSTRACT

An essential aspect of Catenary Anchor Leg Moorings (CALM) buoy structures are the components of hydrodynamics like waves, underwater current, and wind. In this study, numerical investigations on CALM buoy were carried out. Firstly, motion study of free-floating CALM buoy was conducted in ANSYS AQWA. Then an Orcaflex-coupled model of the CALM buoy system with submarine hoses in Lazy-S configuration, was presented. It was attached to six mooring lines under 100 m water depth. Two types of buoy geometries have been investigated: Square Buoy (SB) and the Cylindrical Buoy (CB). Different cases with the same buoy widths were considered using three buoy skirts at 13.90m, 12.90m, and 11.90m. Diffraction analysis was used to obtain the motion behaviour. Results on the CALM buoy motion responses in six degrees of freedom (6DoF) like surge and heave motions, response amplitude operators (RAOs), radiation damping, and added mass, were also presented. The buoy geometry and skirt both influence its hydrodynamics. The study successfully achieved good reports on motion characteristics and wave-current interaction (WCI) for CALM buoys.

1. Introduction

In recent times, there has been an increase in more hydrodynamic studies been carried out numerically and experimentally on different offshore structures. This increase has been necessitated by the advances in computing techniques, climate change effects, deepwater exploration, and adverse weather conditions. Floater structures such as Catenary Anchor Leg Moorings (CALM) buoys with smaller water plane area would have a much different effect from harsh waves than deep draft structures like Semisubmersible hulls (RPSEA, 2009; Zou et al., 2013, 2014, 2017; Amaechi et al., 2021a, 2021b, 2021c, 2021d; Odijie and Ye, 2015a, 2015b), CALM buoys (Ricbourg et al., 2006; Amaechi, 2022; Qi et al., 2017; Ryu et al., 2006; Saito et al., 1980) and TLPs (Chandrasekaran and Jain, 2002, 2007; Jain, 1997). A typical CALM buoy system attached to a floating semisubmersible platform is depicted in Fig. 1. The effect of wave forces on buoys can be significant due to the small water plane area, and this can also affect mooring loads on floater motions. Thus, it is important to carry out a comprehensive hydrodynamics study on the buoy system, to optimise the model by ensuring that the dynamic behaviour of attachments like mooring lines, hawser, marine hoses (submarine hoses and floating hoses) does not distort the stability (Amaechi et al., 2019a, 2019b, 2021e, 2021f, 2021g, 2021h, 2021i). However, since both the CALM buoy and the Paired Column Semisubmersible (PCSemi) are floating offshore structures (FOS) that display six degrees of freedom (6DoF), as shown in Fig. 2, hydrodynamics is vital in the design (Amaechi, 2022, Odijie, 2016; Mohamed, 2011; Odijie et al., 2017a, 2017b).

Wave forces also influence the behaviour of FOS like floating buoys (Edward C. et al., 2021, Amaechi et al., 2019a, 2019b, 2021e, 2021f, 2021g, 2021h, 2021i). Wave forces on offshore structures are computed by applying wave theories, like Airy wave theory. Some components of the FOS's body that influence the waves, including the body's inertial and drag components, are computed using Morison's equation (Morison et al., 1950). Morison's equation does not account for wave diffraction and therefore not sufficient in calculating the wave forces on offshore structures. Diffraction wave theory is typically applied. The complexities associated with the incident, scattered and diffraction wave potentials

* Corresponding author. Engineering Department, Lancaster University, Lancaster, LA1 4YR, UK.,
** Corresponding author.
E-mail addresses: c.amaechi@lancaster.ac.uk, chiemelavic@gmail.com (C.V. Amaechi), j.ye2@lancaster.ac.uk (J. Ye).

https://doi.org/10.1016/j.oceaneng.2021.110378
Received 5 April 2021; Received in revised form 7 December 2021; Accepted 9 December 2021

Abbreviations

ρ	Density of water
ω	Angular frequency
ω_p	- Peak angular frequency
γ	Peak enhancement factor
η	The incident wave amplitude
λ –	Wavelength
θ	Angle to the horizontal axis
2D –	Two Dimensional
3D –	Three Dimensional
6DoF	Six degrees of freedom
a	wave amplitude
A	Area of the body
ABS –	American Bureau of Shipping
CALM	Catenary Anchor Leg Mooring
CB	Cylindrical Buoy
CCA	Chain-Connecting Arm
CCS	Cartesian Coordinate System
C_d	drag coefficient
C_m	Inertial force coefficient
CoG –	Centre of Gravity
δ	hull deformation
DAF –	Dynamic Amplification Factor
DAF_{hose-}	Dynamic Amplification Factor of Hose
DNVGL	Det Norkse Veritas & Germanischer Lloyd
f	wave frequency
FE	Finite Element
FEM	Finite Element Model
FOS	Floating Offshore Structures
FOWT	Floating Offshore Wind Turbine
FPSO –	Floating, Production, Storage and Offloading
g	Gravitational constant
GoM –	Gulf of Mexico
GMPHOM –	Guide to Manufacturing and Purchasing Hoses for Offshore Moorings
H_s	Significant wave height
ID	Inner Diameter
JONSWAP	Joint North Sea Wave Project
MBR	Minimum Bend Radii
MWL	Mean Water Level
OCIMF	Oil Companies International Marine Forum
OD	Outer Diameters
OLL –	Offloading Lines
PCSemi	Paired Column Semisubmersible
PLEM	Pipeline End Manifold
QTF –	Quadratic Transfer Function
RAO	Response Amplitude Operators
s	Arc length
SB	Square Buoy
SPM	Single Point Mooring
T_h –	Horizontal tension force
TLP	Tension Leg Platforms
T_v –	Vertical tension force
T_z	Zero crossing period
V	Volume of the body
W	Weight of the body
WCI –	Wave-Current Interaction
w_s	Submerged weight
x	Section length of the mooring line
z	Height above seabed

have been a subject of discussion in the offshore industry for quite some time, and useful theories have been postulated to resolve some of these problems. Wave forces induce some stress effects, which could lead to high motion predictions, system failures and material failures due to material complexities (Edward and KrDev, 2021; Brown, 1985a, 1985b; Bridgestone, 1976; Berteaux, H.O., 1976). They could also result in high deformations, bending and torsional forces on marine hoses. As such, the need to investigate the motion behaviour of the floating structure based on its hydrodynamics. The hydrodynamic loads are useful in accessing the strength of various offshore structures, hull designs, and components like tubular pipes (Wang et al., 2017a,b; Lenci and Callegari, 2005; Amaechi et al., 2021j, 2019c, 2019d), composite marine risers (Amaechi et al., 2019e,f, Amaechi and Ye, 2017, 2021k–m), and marine hoses (Amaechi et al., 2019a, O'Donoghue & Halliwell, 1988, 1990; Brady et al., 1974). The action of waves are important in the motion and strength behaviour of these CALM buoy hose systems. Basically, FOS operate in ocean environments, as such, their motions are also induced by water waves (Hirdaris S.E. et al., 2014, Bai and Bai, 2005, Berteaux, H.O., 1976, Wilson, J.F., 2003; Brebbia and Walker, 2013; Chandrasekaran, 2015; Sarpkaya, 2014; Faltinsen, 1990). In particular

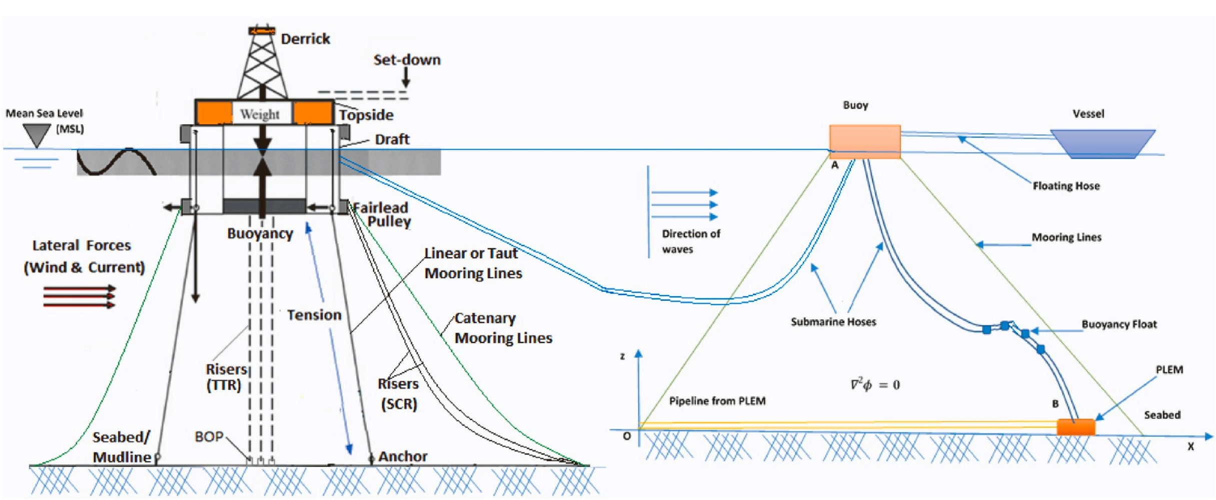

Fig. 1. Sketch of Loading and offloading operation showing a CALM buoy in Lazy-S configuration attached to an offshore platform.

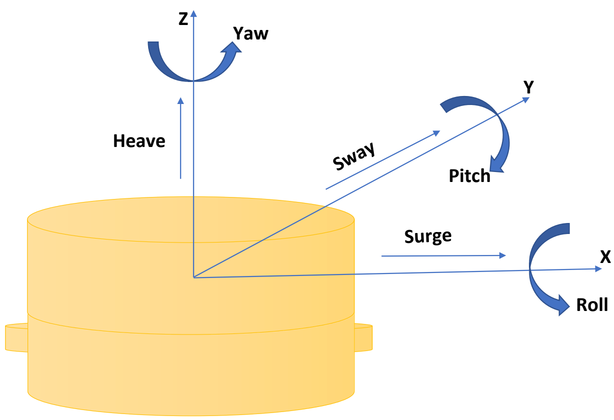

Fig. 2. The six degrees of freedom of a floating CALM buoy.

instances, it induces hose motion (O'Donoghue, 1987; Young et al., 1980; Ziccardi and Robins, 1970; Tschoepe and Wolfe, 1981; Amaechi et al., 2019a), affects CALM buoy motion (Quash and Burgess, 1979; Roveri et al., 2002; Lebon and Remery, 2002; Amaechi et al., 2021h) and other offloading system stability (Amaechi et al., 2021i; Esmailzadeh and Goodarzi, 2001a; Esmailzadeh and Goodarzi, 2001b; Lee and Choi, 2002; Lee and Choi, 2005; Sphaier et al., 2002). Thus, different calculations on wave loads for offshore structures, in general, have been carried out over the years on linear theory (Havelock, 1940; MacCamy and Fuchs, 1954), second order wave forces (Chakrabarti, 1975; Lighthill, 1979, 1986; Newman, 1996; Ghalayini and Williams, 1991) and Morison's equation (Morison et al., 1950; Zhang S. et al., 2015; Liu B. et al., 2020; Kang Y. et al., 2014; Kang Z. et al., 2017). Notably, results from simulations were compared with a coupled CALM buoy model developed in deep water conditions by coupling (Amaechi et al., 2021q–s). Cozijn et al. (2004) found out that applying quadratic absolute velocity on CALM buoys showed that there was better relationship from the CALM buoy model test and the fully coupled model than with the quasi-static simulations. The mooring lines used were modelled using the lumped mass method. Due to the increase in reported CALM buoy failures, there was the need to investigate these further. This led to better estimations such as the quadratic relative velocity (Berhault et al., 2004), the quadratic drag linearization (Salem et al., 2012), and other studies of CALM buoys in Squall condition (Brown et al., 2016, 2017; Duggal et al., 2011; Duggal and Ryu, 2005; Paalvast et al., 2016). Some previous works on buoy skirts have been reported (Edward and KrDev, 2021; Kang et al., 2017; Wang & Sun, 2014, 2015; Ryu et al., 2006; Cozijn et al., 2004, 2005). Wang and Sun (2015) investigated the CALM buoy to determine radiation forces caused by surge, heave and pitch motion in the radiation problem. They concluded that while there is an increase in the radius of the skirt, the added mass in pitch and the added mass in heave will be increased, and the damping coefficients in heave will be decrease. Cozijn et al. (2005) conducted a model test of CALM buoy with skirt scaled at 1:20 obtaining results on the pitch, roll and heave damping which were compared against numerical findings from DIFFRAC using two different skirt dimensions, with results of drag coefficients. Edward and KrDev (2021) presented an investigation using 5 buoy skirt dimensions and found that the skirt has an effect on the heave's RAO, pitch's RAO and roll's RAO and presented the viscous damping of the skirt width for heave. They found that an increase in skirt size reduces the heave RAO, but increase the pitch/roll RAO and increases the viscous damping. Ryu et al. (2006) conducted an experimental validation on a CALM buoy by comparing the effect with and without skirt to derive coupled motion RAOs in frequency domain. For cylindrical bodies like cylindrical FPSO and cylindrical CALM buoys, the hydrodynamic understanding stem from various studies on cylinders and piles. Some offshore structure formulations use theories postulated by Morison on piles called the Morison Equation (Morison et al., 1950). However, due to some limitations, it has been improved upon. Potential theory has also been relatively easier in the estimation of the flow around spheres, buoys and cylinders. In addition, Morison's equation was found to be less accurate in some investigations using linear diffraction theory, as seen in the proposed models by Liu B. et al. (2020) and Zhang S. et al. (2015). They both improved the Morison's equation in the computation of wave loads on floats and floating hoses, respectively, which was more accurate when compared at different water depths. The buoy motion was designed considering studies on buoys (Berteaux, 1976), Vugts, Jan H. 1968) and cylinders (Jacobsen L.S. 1949, Chakrabarti S.K. 1972, 1975; Raman H. & Venkatanarasaiah, 1976, Raman et al., 1977; Garrison, 1974, 1975, 1979, 1984). These have also been used in the determination of the coefficient of added mass, such as 1.5 for CALM buoy hoses (Vugts, Jan H. 1968, Bree et al., 1989; O'Donoghue, 1987). Potential theory was also considered in developing the fluid domain and the wave forces around the submarine hose as an offshore structure (Lighthill, 1979; Rahman and Chakravartty, 1981; and Bhatta and Rahman, 2003; Ghalayini and Williams, 1991). Bhatta and Rahman (2003) considered using differential equations and perturbation method of Lighthill (1979) to develop the boundary conditions, forces and moments of a submarine hose segment using radiation/diffraction theory. (Amaechi et al., 2021a,s) studied the CALM buoy hydrodynamics and proposed a model for strength estimation of CALM buoy submarine hoses based on Orcaflex line elements, and proposed a DAF_{hose} which was applied based on the RAO with and without hydrodynamic loads on the CALM buoy, to estimate the submarine hose behaviour in Chinese-lantern and Lazy-S configurations. Earlier mathematical models on the hydrodynamics of CALM buoys have also been presented (Brown & Elliott, 1987, 1988; Zhang et al., 2015; Bree et al., 1989; Huang and Leonard, 1989, 1990; Brown, 1985a, 1985b). Amaechi et al. (2021t) reviewed the mathematical models on CALM buoy hose systems and portrayed some advances. However, there is still a gap in the understanding of the hydrodynamics of the CALM buoy system, as reported in the Girassol CALM buoy incident of 2002 (Jean P. et al., 2005; Denny D. 2006; Edward C. and KrDev, 2021; Wichers J. 2003). They reported that it was due to premature rupture of the mooring lines attached to the dedicated Girassol CALM buoy for unloading the Girassol FPSO in Angola Field. The mooring chains for the Girassol CALM buoy had only a half-year of service when it occurred as a result of bending-fatigue of the first free chain links inside the chain hawser (fairlead). Albeit, the moorings failed despite that the mooring lines were designed per the offshore industry standards. The bending phenomenon warranted a redesign of the top chain segment and the hawser connection to include a new chain-connecting arm (CCA). Thus, the need for this study as seen with similar investigations on coupled FPSO and/or CALM buoys model (Gu H. 2016; Gu H. et al., 2017, 2019; Le Cunff. 2007, 2008; Kang Y. et al., 2014; Woodburn P. et al., 2005; Amaechi C.V. et al., 2019a), on the motion response (Wang H. et al., 2017b; Sun L. et al., 2015; Amaechi C.V. et al., 2021h, 2021i; Kang et al., 2014), as well as on hydrodynamics of CALM buoy components (Bunnik T. et al., 2002; Cozijn et al., 2004; Duggal, A. & Ryu, S., 2005.; Edward and KrDev, 2021), to better understand the motion behaviour of CALM buoys. Similarly, some recent CALM buoy's hose studies have also been numerically applied at Iran's Petroleum University of Technology (Bidgoli et al., 2017; Hasanvand & Edalat, 2020, 2021a, 2021b, 2021c, 2021b), however, these studies did not consider buoy skirts, buoy dimensions, buoy motions and responses. The studies numerically investigated the dynamics of marine hoses and mooring lines in CALM buoy terminals (Edalat and Hasanvand, 2021a,b, Hasanvand and Edalat, 2020, 2021a–c).

This paper presents CALM buoy motion responses from hydrodynamic studies carried out in ANSYS AQWA R2 2020. Section 2 avows the general problem description, the assumptions considered, and governing equations. Section 3 presents the numerical method, including an Orcaflex coupled model proposed in the design of the CALM buoy system with submarine hoses attached to in Lazy-S configuration. It was moored using six mooring lines under a water depth of 100 m. The numerical model also involved both static and dynamic analysis, and the diffraction analysis was used to obtain the motion behaviour of the Square Buoy (SB) and the Cylindrical Buoy (CB). The effect of the buoy geometry-square and cylindrical shapes, and buoy skirt have some impact on the hydrodynamics of the CALM buoy. Validation was presented in Section 3.7. Results of buoy's 6DoF motions, RAOs, radiation damping, added mass, position response, and waves-current interaction were presented and discussed in Section 4. Conclusion and recommendations on this research were given in Section 5.

2. General description

The general description on the hydrodynamics and statics formulation of the buoy and the attached offshore hoses is presented in this section. Fig. 1 is a sketch of loading and offloading operation showing a CALM buoy in Lazy-S configuration attached to an offshore platform. Some formulation on the theory with governing equations are also included here briefly.

2.1. Problem description

CALM buoys are offshore structures that display 6DoF (six degrees of freedom), as depicted in Fig. 2. They are also used in ocean environments and their motions could be induced by water waves (Amaechi et al., 2021m,n,p,q). This study focuses on the motion performance of the CALM buoy system depicted in Figs. 1 and 2.

2.2. Assumptions

The system is considered to be a floating CALM buoy, with the attached components. These include the floating hoses, submarine hoses, the hawsers and the mooring lines. The buoy is also considered as a single system with rigid body of 6 DoFs, as shown in Fig. 2. The following are assumed:

1. Wave diffraction effects are neglected.
2. The seabed is horizontal and on a rigid plane.
3. The fluid is incompressible, irrotational and bounded by the free surface, rigid bottom and surface of the buoy.
4. Wave loads effects from transport vessels like FPSO are negligible as assumed to be.
5. Wave forces acting via the mooring lines are negligible as assumed to be.
6. The mooring cables, the moorings and the mooring lines mean the same thing in this study.
7. At equilibrium, the initial pre-tension in the mooring lines are equal and constant over time. However, this is subject to the motion response of the CALM buoy.
8. For every time step considered, the solution for changes in pretension were carried out so that during each time step, the equations of equilibrium also reflect the changes in the stiffness matrix's elements.
9. Both the low frequency drift along the surge motion cum the oscillations of the high frequency tension generated by the mooring lines attached to the buoy are not considered in the analysis of the buoy.

2.3. Governing equations

Application of Morison's equation in studying waves on the CALM buoy is important in understanding the motion behaviour (Sorensen, 1993, 2006; Sarpkaya, 2014; Berteaux, 1976). These wave forces are a direct function of the fluid phase pressure 'P_θ' exerted on the body, as seen Equations (1) and (2).

$$P_\theta = \frac{H}{2}\,(P_r \cos\theta + P_i \cos\theta) \tag{1}$$

Where the subscripts r and i represent the real and imaginary components of the pressure, H is the wave height and θ is the flow angle.

$$F_i = \iint_{s_w} P_\theta \vec{n_j}\;\mathrm{d}S = -\rho \iint_{s_w} (j\omega\varphi + gz)\vec{n_j}\;\mathrm{d}S \tag{2}$$

F_i is the first order pressure force, s_w is the wetted surface, $\vec{n_j}$ is the normal (a unit vector) component of the wetted surface vibration mode, z is the height of the submerged hull length, ω angular velocity, g is gravity, ρ fluid density, φ wave complex potential which can be expressed as

$$\varphi = \varphi_i + \varphi_s + \sum_{j=1}^{6}\varphi_r \tag{3}$$

Where the terms φ_i, φ_s and φ_r are the incidence, scattered and radiation wave potentials respectively, and j represent the mode of vibration of the body.

Submarine hoses are slender bodies, so in this study, the damping is calculated using the following modified Morison Equation (Morison et al., 1950) in Equation (3), where V is the volume of the body, A is the area of the body, D is the diameter of the body, C_d is the drag coefficient, C_a is the added mass coefficient, C_m is the inertial force coefficient, and the V_r is the relative velocity of fluid particles.

$$F = \rho V\dot{u} + \rho C_a DA(V_r) + \frac{1}{2}\rho C_d A(V_r)|V_r| \tag{4}$$

However, considering the wave theory used to obtain the potential's relationship in Equation (3), the Navier Stokes equation can be applied for incompressible fluid acting in irrotational motion under a sea depth h, on a floating buoy of depth, d (Amaechi et al., 2021i,s,t, Lighthill, 1979, 1986, Rahman, 1981, 1984; Rahman and Chakravartty, 1981). The velocity potential can be expressed as:

$$\varphi(x,y,t,z) = \varphi(x,y)f(z)e^{i\omega t} \tag{5}$$

$$\nabla^2\varphi = 0 \tag{6}$$

Considering diffraction theory, impermeable cases are without normal flux or normal velocity as given in Equation (7), thus, it can be reduced to a 2D problem, in terms of the velocity potential φ(x,y) as:

$$\nabla\varphi.\vec{n} = \frac{\partial\varphi}{\partial n} = 0 \tag{7}$$

However, the force on the submarine hose element, F can be deduced using polar coordinates (r,Θ,z) or Cartesian coordinates (x,y,z). Considering Fig. 3, the total force will be a function of the pressure of the fluid, the sea depth and the angle made by the hose element. Thus,

$$\vec{F}(\omega) = -P\cos\theta dS;\; -P\sin\theta dS \tag{8}$$

$$\vec{F}(\omega,t) = -\int_S P\vec{r}dS \tag{9}$$

$$\vec{F}(\omega,t) = -\int_0^{2\pi}\int_{-d}^{0} P\vec{r}.rd\theta dS \tag{10}$$

For a sea depth, z, the force per unit length at the depth where the surface of the buoy element is S (Brebbia and Walker, 2013; Sparks, 2018; Chandrasekaran, 2015; Sarpkaya, 2014; Dareing, 2012).

$$\vec{F}(z,\omega,t) = -\int_0^{2\pi} P\vec{r}.rd\theta \tag{11}$$

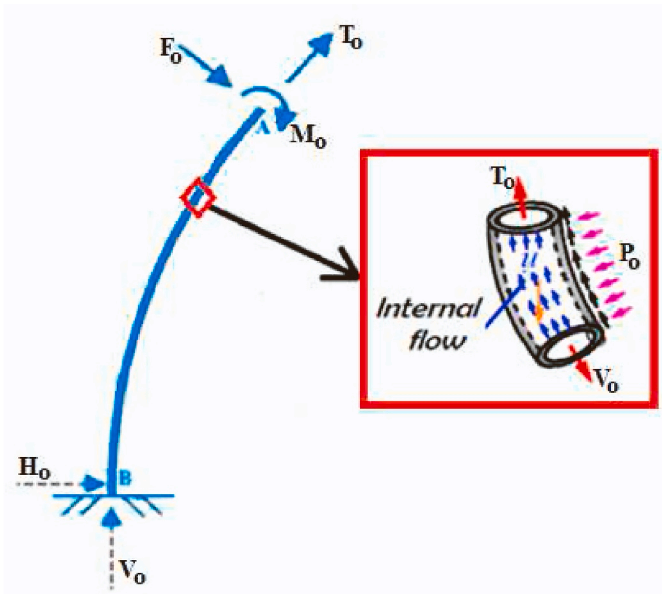

Fig. 3. Schematic of short segment of riser-hose string's stress joint.

It is feasible to derive the governing differential equations for marine hoses from existing equations for marine risers in fundamental literature (Sparks, 2018; Dareing, 2012) such as cable's catenary equations (Luongo and Zulli, 2013; Bai and Bai, 2005). Let us consider a short segment of the hose-string, as shown in Fig. 3, which lies on the arc length, s, the resultant force, T_0, and placed at point A. The horizontal force, H_0, originates from the Cartesian Coordinate System (CCS)'s origin, O, and the vertical force, V_0. At the top section, the external force, F_o acts on the hose string while external pressure P_o, acts on the body of the hose. Since the hose string's speed is variable for each time period, it will make distinct angles between the hose string's axis and the horizon, $\Theta_{(i\,=\,1,2,3,..n)}$; where n is the number of times it uses to complete a full wave cycle, while Θ_0 is the angle formed by the horizontal and the direction of the resultant force. Therefore, as presented by Bishop and Johnson (2011), the equation of motion in Equation (12) exists, where the load, Q, is determined by the hose's weight, w, and the hose's radius, r, which is determined by the water depth, h, and the bending stiffness of a general section of hose, EI_z.

$$EI_z\frac{\partial^4 y}{\partial x^4}+m\frac{\partial^2 y}{\partial t^2}=Q \tag{12}$$

3. Numerical modelling

The numerical modelling approach, the methods and the materials utilised are presented herein.

3.1. Materials and methods

The materials and methods used are described in this section. Fig. 4 is definition of the coordinate system of the CALM buoy hull model. The methodology for the numerical study includes four (4) main steps on the numerical model. It was achieved by first conducting motion response study on the CALM buoy. Then the motion response studies on different buoy geometries by comparing the square buoy (SB) and the cylindrical buoy (CB), with parameters as given in Section 3.8. The proof of concept was done by comparing it with typical CALM buoy using Bluewater's turret buoy (Bluewater, 2011). Next was to perform the motion response studies on different buoy skirts using cylindrical buoy with the same width of 10m in diameter. Then, to include the coupled model, Orcaflex was then used. It was conducted by coupling the hydrodynamic analysis of the CALM buoy in ANSYS AQWA into the Orcaflex model. This is done using a free-floating buoy in ANSYS AQWA to obtain the RAO, added mass and radiation damping. However, flow direction was important in this model, as illustrated in Fig. 4. The development of the numerical procedure was carried out in two phases; hydrodynamic or diffraction analysis and finite element analysis. Fig. 5 shows a schematic sketch of the numerical procedure. The fluid hydrodynamic pressure and response amplitude operator are computed for at different phase angles and generated in a text file (script with FORTRAN programming language using ANSYS APDL) using the beta mode of ANSYS AQWA 2020 R2, which was then used for loading in the FEM. In obtaining the RAOs, the mooring lines and hoses are not included in the ANSYS AQWA model. The need of using a numerical model including mooring lines and hoses in the Orcaflex model is to investigate on the submarine hoses. The diffraction analysis was used to obtain the RAOs and other hydrodynamic parameters for the free-floating buoy. However, it does not exist as free floating in practice else it would drift away from shore or off its position. Thus, the mooring and hoses both affect the RAOs and hydrodynamic coefficients, which is very important. They help to hold the CALM buoy and keep it in position as supporting attachment components. However, the justification of neglecting this effect in the ANSYS AQWA diffraction analysis is that it saves computational resources, as the elements needed will be reduced. Secondly, the mooring lines, marine risers, and marine hoses are slender bodies that may have distorted elements in the hydrodynamic model; otherwise, they could be designed using Morison's elements or line elements or similar techniques. For the buoy motion, considerations were made in the design by considering studies on buoys (Berteaux, 1976; Vugts, Jan H. 1968; Amaechi et al., 2019a, 2021i, 2021s; Tschoepe and Wolfe, 1981) and cylinders (Jacobsen L.S. 1949; Chakrabarti S.K. 1972; Raman H. & Venkatanarasaiah, 1976; Koterayama W. 1984; ITTC, 1987; Demirbilek and Gaston, 1985; Venugopal et al., 2006, 2009). Since the floater behaviour is represented by the RAOs with buoy hydrostatics in Table 4, the motion characteristics from the RAOs generated were loaded into the Orcaflex model (Orcina, 2014, 2020, 2021; Amaechi et al., 2019a). The validation is conducted in Section 3.7 and the verified Finite Element Model was then used in the CALM buoy system numerical modelling and analysis in Section 4, and the results are presented in Section 5.

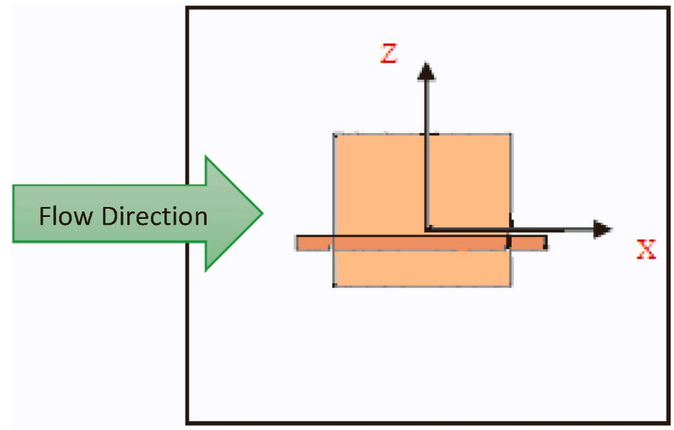

Fig. 4. Schematic for defining the coordinate system of the CALM buoy hull.

3.1.1. Buoy

The buoy parameters applied in the design analysis are presented in Table 1. The buoy model used in the diffraction analysis is a free-floating buoy in ANSYS AQWA. However, the model was later attached with two submarine hoses attached underneath the buoy in the Orcaflex model interface, as shown in Fig. 6. DNVGL (2017) specifies the global performance for FOS like the floating buoy and FPSO.

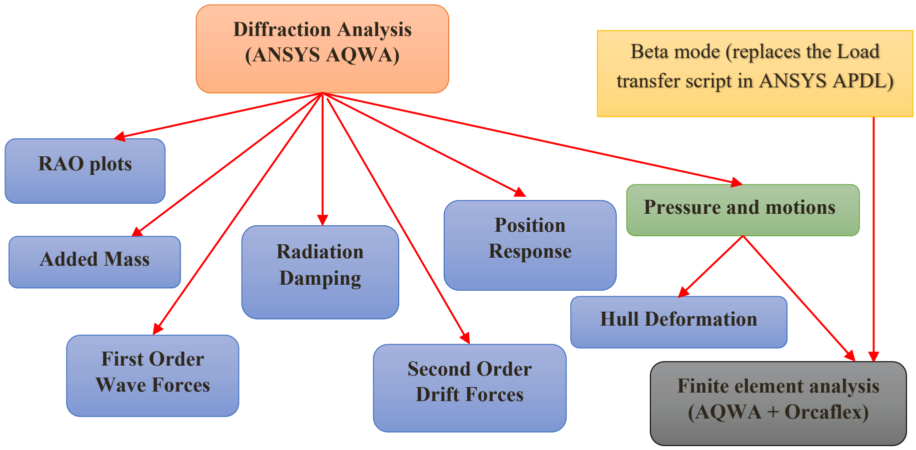

Fig. 5. Schematic diagram of numerical analysis and coupling model.

Table 1
Buoy parameters.

Particulars	Value
Height (m)	4.4
Draft size (m)	2.4
Main body diameter (m)	10.0
Skirt diameter (m)	13.870
Water Depth (m)	100
Buoy Mass (kg)	198,762

3.1.2. *Hose*

In this model, both the submarine and the floating hoses were used. However, the submarine hoses were considered particularly due to their applications underneath the buoy, as illustrated in Fig. 1. Two submarine hose strings are connected to the base of the buoy at the top and the Pipeline End Manifolds (PLEMs) at the bottom. The outer and inner diameters of the hoses are 0.650 m and 0.490 m, respectively, as detailed in Table 2. The pressure rating was for 1,900 kN/m^2 (19 bar) application. The Orcaflex 3D view of the CALM buoy model in Lazy-S configuration, showing the ocean environment, is presented in Fig. 17. The submarine hose model for the CALM buoy has already been validated by the authors in literature (Amaechi C.V. et al., 2019a, 2019b). The design of the hoses is carried out using the simple beam theory in the statics, and then simulated in Orcaflex using the line theory. By current industry practice, the marine hose should be designed according to OCIMF (2009, 1995a, 1995b, 2020). In prinicple, detailed hose investigations are important from local design to global design (Amaechi, 2022; Amaechi et al., 2021m,n,p–r).

3.1.3. *Floats*

Buoyancy floats were used in designing for the buoyancy force of the hoses by using floats integrated at selected locations on the hose string, as illustrated in Figs. 7 and 11. The main lines of the submarine hoses used in the design were designed without float collars, by using standard floats attached to these hoses. The parameters for the float are given in Table 3, based on industry specifications (ABS, 2014; API, 2013, 2017, 2021; OCIMF, 2009; Yokohama, 2016; Trelleborg, 2017). The floats were considered in the dynamic analysis in Orcaflex to reduce the bending moment on the buoyant marine hoses, by providing additional buoyancy support.

3.1.4. *Mooring lines*

In the model, the mooring lines are an important part of the CALM buoy system. The mooring line is made of polyester wire and steel chain. It is designed using industry guidelines on mooring lines, position moorings, and single point mooring (SPM) systems (ABS, 2021, 2011; API, 2014, 2005; DNV, 2013; DNVGL, 2015, 2016). Each mooring line contributes to the load effect of the system for its relative position, velocity and acceleration. The statics calculation of the mooring lines was carried out using the catenary method (Bai and Bai, 2005; Irvine, 1981; Luongo and Zulli, 2013; Wichers, 2013), as shown in Fig. 8. Typical calculation carried out on the mooring lines is presented in Table 4. The catenary equation used is given in Equation (13), where x (or s) is the section length of the mooring line, H (or T_H) is a constant that represents the horizontal tension component, T_v is the vertical tension component, and w is the weight per unit length.

$$y = \frac{H}{w}\left[\cosh\left(w\frac{x}{H}\right) - 1\right] \tag{13}$$

The CALM buoy system was moored with two sections of steel chain moorings. The mooring arrangement was made up of six (6) mooring lines modelled as catenary mooring lines. The mooring lines have the same stiffness and were 60° apart, with details in Table 5. One end of the mooring line was attached to the skirt of the cylindrical buoy, while the other end was anchored to the seabed, as represented in Figs. 9, 10 and 17.

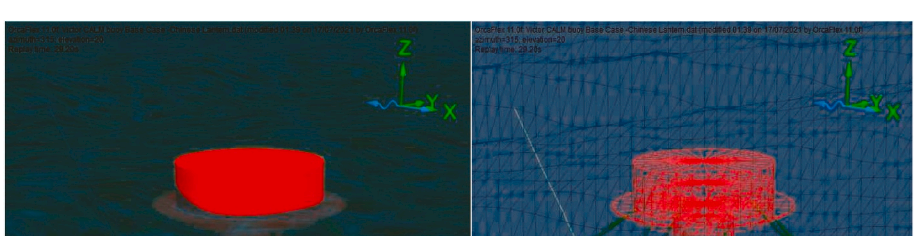

Fig. 6. CALM Buoy Model with skirt in Orcaflex 11.0f, showing shaded and wireframe views.

Table 2
Arrangement for 3 sections of the Submarine Hose.

Parameters	Arrangement	Value
Section 1		
Description	First-off Buoy with Float collars	
Bending Stiffness (kNm^2)	R1 (fitting)	10,000
	R1 (reinforce end)	120
	R1 (body)	78
	R1 (fitting)	10,000
Length (m)		8.39
Mass property (kg/m)		239
Hose Bore (m)		0.490
Section 2		
Description	Mainline without Float collars	
Bending Stiffness	R2 (fitting)	10,000
	R2 (end)	98
	R2 (body)	78
	R2 (end)	98
	R2 (fitting)	10,000
Length (m)		9.02
Mass property (kg/m)		495
Hose Bore (m)		0.490
Section 3		
Description	First-off PLEM with Float collars	
Bending Stiffness	R3 (fitting)	10,000
	R3 (end)	98
	R3 (body)	78
	R3 (reinforce end)	120
	R3 (fitting)	10,000
Length (m)		8.49
Mass property (kg/m)		239
Hose Bore (m)		0.490

3.2. Hydrodynamic panel model

In this study, two different geometries were considered for the hydrodynamic study-cylindrical and square geometries. The hydrodynamic panel model of the Cylindrical Buoy (CB) and the Square Buoy (SB) is presented in Fig. 11. They were developed with ANSYS AQWA R2 2020, which applied radiation diffraction theory. The global performance and hydrodynamic loading of the floating buoy structure were designed in accordance with industry's specification as recommended within DNVGL-RP-C205 (DNVGL, 2017), API RP 2SK (API, 2005) and DNVGL–OS–E403 (DNVGL, 2015, 2016).

3.3. Hydrodynamic damping

The hydrodynamic damping on this study carried out with irregular wave. The modified Morison Equation was considered in the calculation of the damping of the buoy with respect to the earth and considered in the Damping Matrix from ANSYS AQWA (ANSYS, 2017a; 2017b). For the Submarine hoses which are slender bodies, the damping is calculated using the following modified Morison Equation (Morison et al., 1950; Sarpkaya T. 2014; Wilson J.F. 2003), in Equation (4).

For the buoy, the Morison's equation was also applied in this study as given in Equation (4) to discretise the model. The finite element model (FEM) in Orcaflex solver discretizes the CALM buoy model into four (4) main Morison Elements, as shown in Fig. 12. In addition, the buoy's skirt was designed as solid with a smaller diameter to accurately reflect its

Table 3
Float parameters.

Parameters	Value
Type of Float	Standard bolted-type float
Design Depth (m)	40
Weight in Air (kg)	102
Net Buoyancy (kg)	280
Outer Diameter (m)	1.23
Inner Diameter (m)	0.799
Float Depth (m)	0.6
Shell Material	Polyethylene
Filling Material	Polyurethane foam
Metal Part Material	Stainless Steel

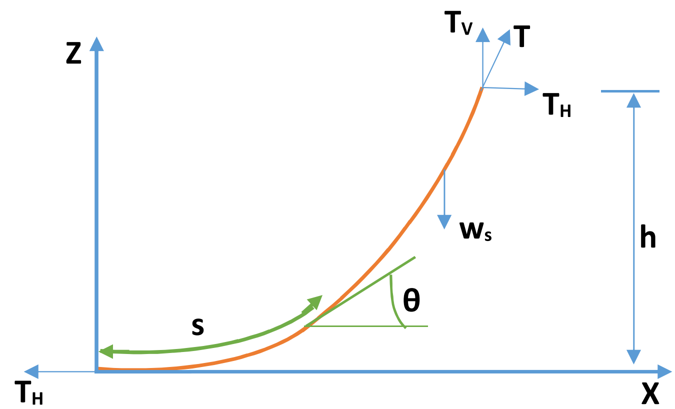

Fig. 8. Schematic of forces on the Catenary design of a mooring line in static mode.

Table 4
Typical Calculation for Mooring line tension.

Calculation:

Known:
The equivalent density (w_s) of hose per unit length in air = 4789 kg/m,
The submerged weight per unit, (w_s) is 5315 kg/m.
Depart angle θ at the top = 30°,
Depart angle θ at the TDP = 45°,
Height above seabed, h of the hose = 1.495m

Calculations:
Top:w_s = 5315 kg/m; θ = 30°; z = 1.495m

Horizontal force $T_H = \frac{z\cdot w_s}{(\tan\theta)^2}\cdot 1 + \sqrt{1 + (\tan\theta)^2}\Big)\Big) = 51363.267\text{kg}$

Arclength $s = h\cdot\sqrt{\left(1 + 2\cdot\frac{T_H}{h\cdot w_s}\right)} = 5.579\text{m}$

Vertical force $T_v = w_s\cdot s = 29652.385\text{kg}$

Touch down point(TDP):
Where w_s = 5315 kg/m; θ = 45°; z = 0m

Horizontal force $T_H = \frac{z\cdot w_s}{(\tan\theta)^2}\cdot 1 + \sqrt{1 + (\tan\theta)^2}\Big)\Big) = 0\text{kg}$

Arclength $s = z\cdot\sqrt{\left(1 + 2\cdot\frac{T_H}{h\cdot w_s}\right)} = 0\text{m}$

Vertical force $T_v = w_s\cdot s = 0\text{kg}$
If the acceleration of gravity:g = 10N/kg,
Top: T_H = 513.63267KN; T_v = 296.52385KN
TDP: T_H = 0KN; T_v = 0KN

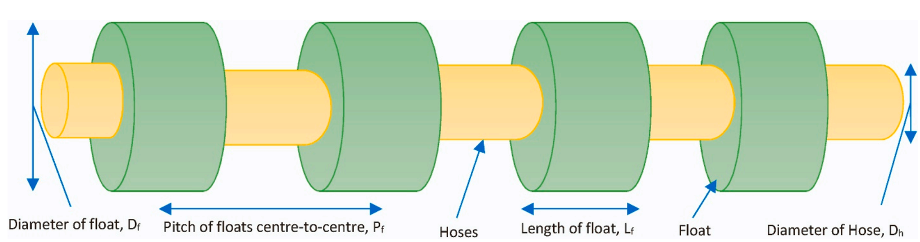

Fig. 7. Typical floats attached to submarine hoses.

Table 5
Mooring lines parameters.

Parameters	Value
Contact Diameter (m)	0.229
Nominal Diameter (m)	0.120
Ratio of Section Lengths	150:195
Mass per unit length (kN/m)	0.088
Poisson Ratio	0.5
Mass coefficient, C_m	1.0
Drag coefficient, C_d	1.0
Bending Stiffness (kN)	0.0
Axial Stiffness, EA (kN)	407,257

effective zone, which is detailed in Table 6. The drag coefficients (C_d) used in the numerical model were not assumed but computed using a semi-empirical calculation in literature (Amaechi, 2022). They were obtained from validated studies on CALM buoys by MARIN and SOFEC (Le Cunff et al., 2007; Cozijn et al., 2004, 2005; Ryu et al., 2006; Duggal and Ryu, 2005). For the polyester mooring lines and hose ends, the C_d value used is 1.0. For the hose body with floats and the hose flanges, the C_d value used for was 1.2, while the C_d value used for modelling the chain mooring lines was 1.18.

3.4. Environmental load conditions

This study employs five (5) different environmental conditions. In this study, the linear theory for the spectral components is used in the simulation of the sea state. The simulations are run using irregular waves for 3 h duration. The JONSWAP (Joint North Sea Wave Project) wave spectrum was adopted in the numerical analysis using a peak factor, γ of 3.3 for all the sea states, as shown in Fig. 13. The main parameters including zero-up-crossing period T_z, significant heights H_s, and peak period T_p, are presented Table 7. These environmental conditions used for the study were applied on the hydrodynamic panels in Fig. 13. It should be noted that the plot was prepared applying the same period approach (Rueda-Bayona et al., 2020; Lucas and Guedes Soares,

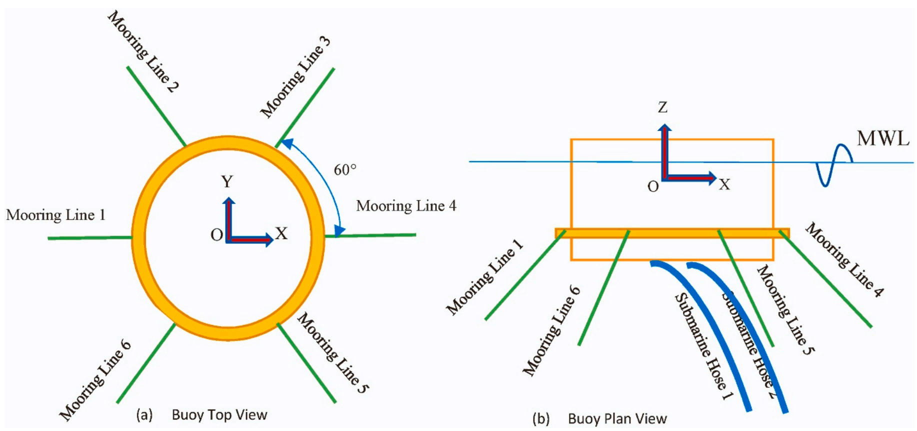

Fig. 9. Local Coordinate System for Buoy and Mooring Lines in (a) buoy top view (b) buoy plan view.

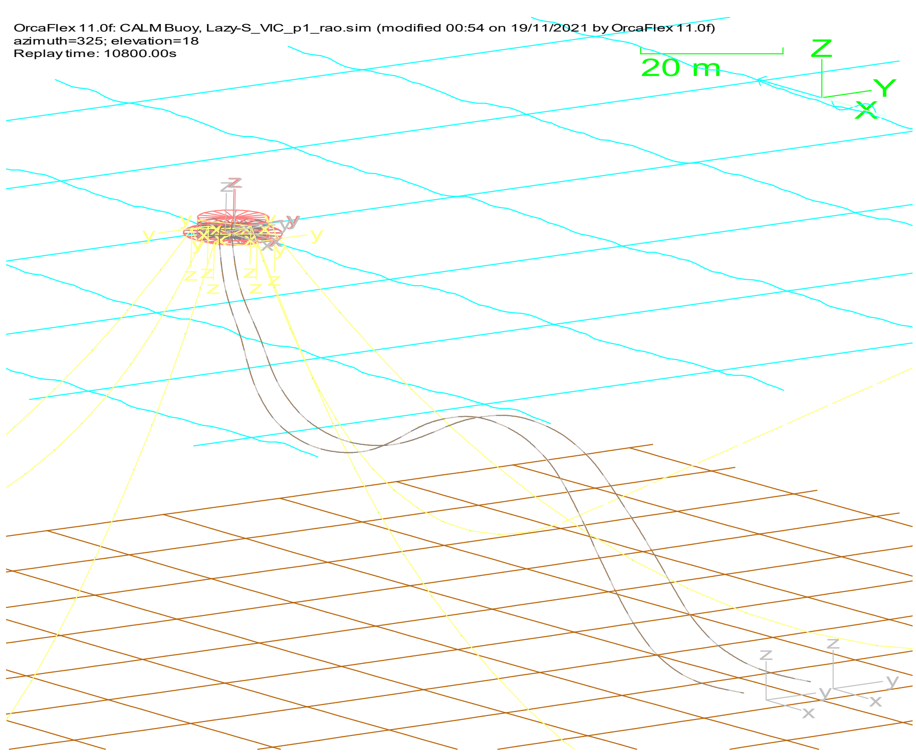

Fig. 10. Orcaflex wireframe model showing the CALM buoy (in red), six mooring lines (in yellow) and two submarine hoses (in grey) in Lazy-S configurations.

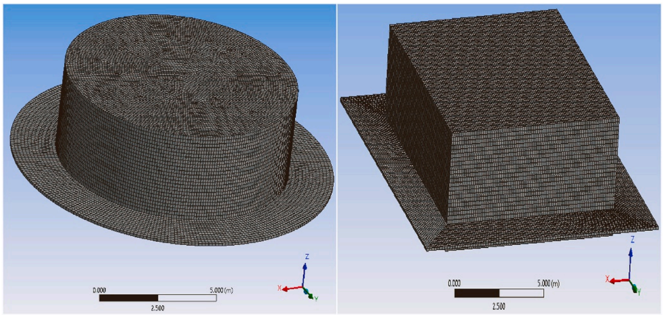

Fig. 11. Hydrodynamic Panel for CALM Buoys in ANSYS AQWA, for the Cylindrical Buoy (CB), and the Square Buoy (SB), respectively.

2015; Rodri'guez, G. & Guedes Soares, C. 1999), but application details utilised are based on the data in Table 7. In this study, the environmental data was considered for deep water in Gulf of Mexico (GoM), so we used API 2-INT MET (API, 2007) using ITTC recommendations on waves (ITTC, 2002, 1987).

3.5. *Wind, current, ocean and seabed modelling*

The environmental conditions in Section 3.4 were considered under irregular waves. The ocean conditions considered in this model as shown in Fig. 17, were under wind, waves and currents. Wind is also considered with a wind speed of 22 m/s. Fig. 14 presents the profiles for the (a) current load coefficients and (b) wind load coefficients of the CALM buoy model. For the seabed, an elastic seabed model was considered. The detailed particulars for the wind, current, seabed and the ocean are tabulated in Table 8. The calculation of the soil friction is not included in this paper, but it is calculated using seabed theory (Orcina, 2014, 2020, 2021). Secondly, the value is validated from existing technical reports on soil modelling and soil friction (Amaechi et al., 2021e; Amaechi et al., 2021m). In this modelling, the current speed for the seabed has been selected based on a parametric study, due to low gradient or slope of the seabed but it is relatively high at 0.45 m/s. Detailed investigation on the effect of the current are presented in Section 4.2. In this study, the wind direction is 0°, and it is collinear (same direction) with the waves in all the runs. The current profile utilised for the numerical modelling in Fig. 15(a and b) shows 3D vertical profile at seabed origin using 0.5 m/s surface current and 0.45 m/s seabed current.

3.6. *Orcaflex Line finite element model*

Orcaflex applies line theory, where lumped mass model is used for mooring lines, as shown in Fig. 16. For submarine hoses, it applies lines, which are considered as massless with distributed concentrated mass. In principle, the line element support flexibility of the line to have axial displacement, torsion, tension and bending. Details on the principle of line theory used in the FEM of the submarine hose lines and the mooring lines in Orcaflex are represented in Fig. 16. The model as presented in Figs. 10 and 17 was developed using the details in Sections 3.1-3.5. The Finite Element (FE) model presented in Fig. 17 shows the submarine hoses, CALM buoy, mooring lines, seabed and boundary conditions for the CALM buoy in Orcaflex version 11.0f. The CALM buoy is floating on an ocean acted upon by waves, currents and other hydrodynamic forces.

3.7. *Validation*

The Orcaflex dynamic models are expected to be capable of performing dynamic analysis on the hose in centenary configuration. Using the verified static models, the dynamic effects provided by Orcaflex was studied on catenary S-lay pipeline via recently established sea trial tests (Wang F. et al., 2017a), Lazy-S configured marine hoses (Amaechi et al., 2021s) and Chinese-lantern configured marine hoses (Amaechi C.V.

Table 6
The damping coefficients of the CALM buoy.

Description	Undersurface Coordinate			D (m)	H (m)	C_d
	X (m)	Y (m)	Z (m)			
Morison Element 1	0	0	0	10.00	1.70	1.00
Morison Element 2	0	0	0.9	10.00	1.70	1.00
Morison Element 3	0	0	1.0	13.87	0.10	1.10
Morison Element 4	0	0	2.7	10.00	0.90	1.00

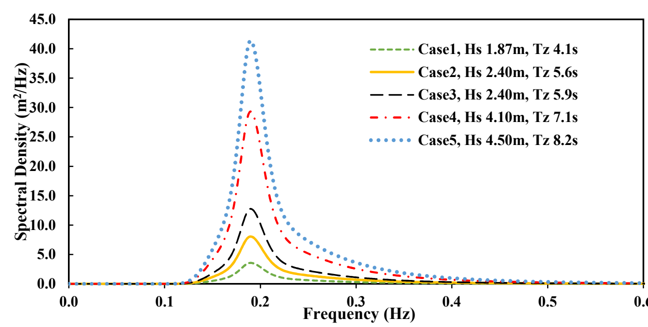

Fig. 13. JONSWAP Spectrum for the 5 Sea States or Environmental Cases, where Case 1 is normal wave state while Case 5 is extreme wave state.

Table 7
Wave Parameters for the 5 load Cases.

Case No.	H_S (m)	T_Z (s)	T_P (s)
1	1.87	4.10	5.27
2	2.40	5.60	7.20
3	2.40	5.90	7.56
4	4.10	7.00	9.00
5	4.50	8.20	10.55

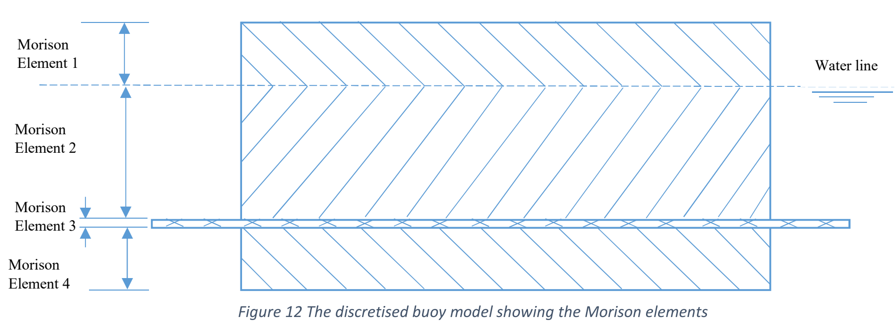

Fig. 12. The discretized buoy model showing the Morison elements.

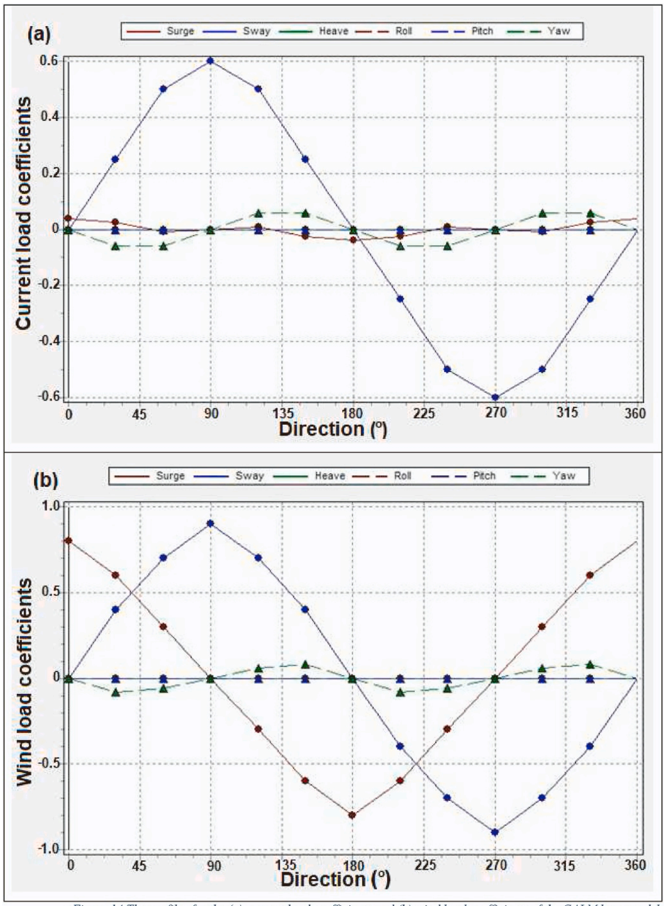

Figure 14 The profiles for the (a) current load coefficients and (b) wind load coefficients of the CALM buoy model

Fig. 14. The profiles for the (a) current load coefficients and (b) wind load coefficients of the CALM buoy model.

Table 8
Wind, current, ocean & seabed parameters.

Parameter	Value
Water Density (kgm^{-3})	1,025
Ocean Kinematic Viscosity (m^2s^{-1})	1.35 X 10^{-6}
Wave Amplitude (m)	0.145
Seabed Stiffness ($kNm^{-1}m^2$)	7.5
Ocean Temperature (°C)	10
Water Depth (m)	100.0m
Seabed Friction Coefficient	0.5
Seabed Shape Direction (°)	0
Seabed Model Type	Elastic Linear Model
Wind Speed (ms^{-1})	22.0
Air Density (kgm^{-3})	1.225
Air Kinematic Viscosity (m^2s^{-1})	0.000015
Current Direction (°)	180
Surface Current (ms^{-1})	0.50
Seabed Current (ms^{-1})	0.45
Wind Direction (°)	0

et al., 2019a). On this present model, the validation results from both the finite element analysis and the analytical calculations are presented in Table 9. The results of the finite element analysis (FEA) and analytical computations for horizontal tensions were 115.40 kN and 109.30 kN respectively. The results of the FEA and analytical computations for vertical tensions were 78.50 kN and 81.60 kN respectively. This shows good agreement between both approaches with variations of 5.30%, and 3.90% respectively, across both horizontal and vertical forces.

An extensive mesh convergence analysis in the diffraction study in ANSYS AQWA R2 2020 was conducted to validate the numerical model.

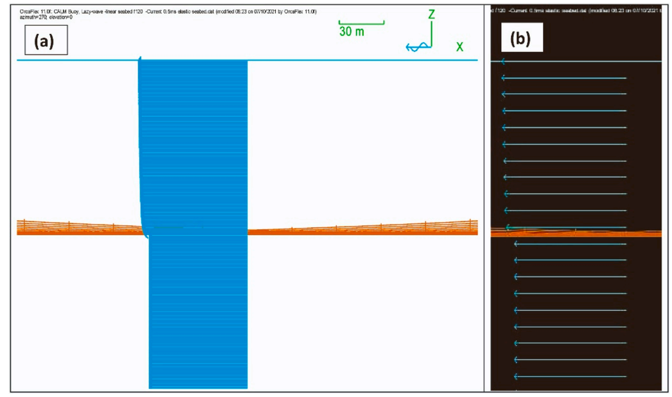

Fig. 15. The profiles for the current showing its 3D vertical profile at seabed origin for 0.5 m/s surface current and 0.45 m/s seabed current, in (a) 3D shaded view and (b) wireframe view, in Orcaflex 11.0f.

The model was developed using boundary element method (BEM) as it has its advantages over finite element method (Newman and Lee, 2002; Brebbia and Dominguez, 1977, Ye, 1988; Amaechi et al., 2021i). Some of these BEM models have been validated using numerical and experimental methods (Wang H. et al., 2017b; Wang F. et al., 2017a; Pinkster and Remery, 1975, Ricbourg et al., 2006; Kim and Sclavounos, 1998). In the present model, a tolerance of 0.01m and the maximum element size of 0.25m were considered. In order to ensure that the effective mesh density was obtained, the range of the elements was from 1.25m to 0.25m. The convergence study was carried out using the panel model of the CALM buoy under ocean environment to study the tension, surge displacement and bending in the surge motion. The RAO values were obtained from the hydrodynamic parameters such as potential damping and added mass. Table 10 shows the results obtained from the effect of the maximum surge RAO that acts along the 0° incidences. The study showed that there were very small deviations in the RAOs obtained from the maximum at 0.25m element size. Precisely, it is very less minimal, and very much less than 4%, which means that the tolerated deviation considered in this analysis will save computational resources and also be sufficient, acceptable, and validates this study.

3.8. Buoy geometries and buoy skirts

The motion response of the CALM buoy was carried out and is presented in this Section 4. This research also presents a comparative study between both square buoy (SB) and cylindrical buoy (CB), to present the advantage and justification. Its application includes aiding designers in considering some skirt parameters. The descriptive illustration of the buoy geometry is given in Fig. 16. It shows the diameters, radius, angles and positions of each part. It was comparatively investigated for three different skirts with the same buoy width, as tabulated in Table 11 and shown in 19. In this study, two (2) geometries-cylindrical buoys (CB) and square buoys (SB), are used, as seen in Figs. 18 and 19. The description of the cylindrical buoy (CB) with its CALM buoy's skirt, as depicted in Fig. 18, also includes the CALM buoy's body diameter D_B and the CALM buoy's skirt diameter D_S. The tangential position around the skirt's circumference is defined by an angle, α. (14) and (15) are used to determine the skirt's dimensions concerning the cylindrical buoy (CB), and square buoy (SB) using diameter (D) for CB, and cross-sectional length (L) for SB, thus;

$$D = \frac{D_S}{D_B} \tag{14}$$

$$L = \frac{L_S}{L_B} \tag{15}$$

Where CB's CALM buoy's body diameter D_B, CB's CALM buoy's skirt

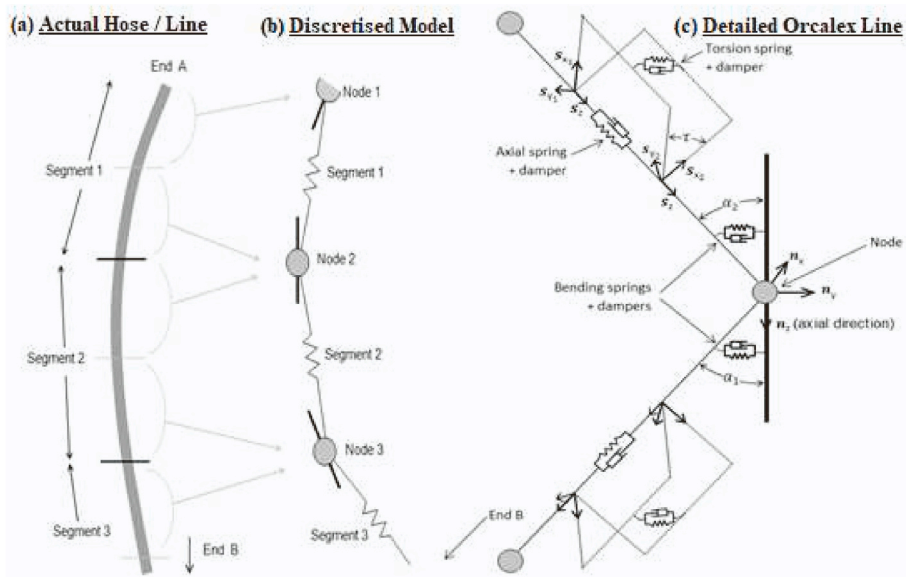

Fig. 16. Orcaflex Line Model showing (a) the main line, (b) the discretized model and (c) nodes with spring and dampers (courtesy of Orcina, 2014, 2020, 2021).

Fig. 17. CALM buoy model in Lazy-S configuration, showing the ocean environment in Orcaflex 11.0f.

Table 9
Validation results for hose maximum tensions in horizontal and vertical components.

Parameters	Horizontal Tension (KN), T_h	Vertical Tension (KN), T_v
Analytical Model (Hand Calculation)	109.30	81.60
Finite Element Model (FEM in Orcaflex)	115.40	78.50
Averaged Ratio (Analytical/Finite Element)	0.947	1.039

Table 10
Mesh Grid independence for Surge Study using diffraction analysis.

Element Size (m)	No. of Nodes	No. of Elements	Max. Surge RAO (m/m)	Max. RAO Deviation on 0.25m
1.25	1144	1113	1.18470	0.0827%
1.0	1632	1593	1.18540	0.0556%
0.5	5564	5489	1.18627	0.0187%
0.35	10728	10623	1.18650	0.0099%
0.25	20303	20156	1.18664	0.0000%

Table 11
Table showing CALM buoy skirt diameters considered.

CALM buoy Skirt Cases	Buoy Geometries	Skirt Diameter, D_s (m)	Buoy Diameter, D_b (m)	Diameter Ratio, $D = D_s/D_b$
Skirt 1	Cylindrical Buoy (CB)	13.90	10.0	1.39
Skirt 2	Cylindrical Buoy (CB)	12.90	10.0	1.29
Skirt 3	Cylindrical Buoy (CB)	11.90	10.0	1.19
CALM buoy Skirt Cases	Buoy Geometries	Skirt Length, L_s (m)	Buoy Length, L_b (m)	Length Ratio, $L = L_s/L_b$
Skirt 1	Square Buoy (SB)	13.90	10.0	1.39
Skirt 2	Square Buoy (SB)	12.90	10.0	1.29
Skirt 3	Square Buoy (SB)	11.90	10.0	1.19

diameter D_S, SB's CALM buoy's body cross-sectional length L_B, and SB's CALM buoy's skirt cross-sectional length L_S.

3.9. Hydrostatic properties

The parameters for the buoy hydrostatics are presented in Table 12. The details for the other hydrostatic properties are given in Tables 13–15. This includes the hydrostatic stiffness, added mass matrix, and damping matrix, respectively. These are essential parameters but different from the RAO values obtained from the hydrodynamic investigation. Fig. 20 depicts the model view of the CALM buoy in the free-floating mode for the hydrodynamic and hydrostatic analysis. The X and Y direction of the sea were represented using this model box of 150m × 150m that replicates the fully developed sea condition.

4. Results and discussion

In this section, the results from the numerical studies on the motion response of the CALM buoy are presented.

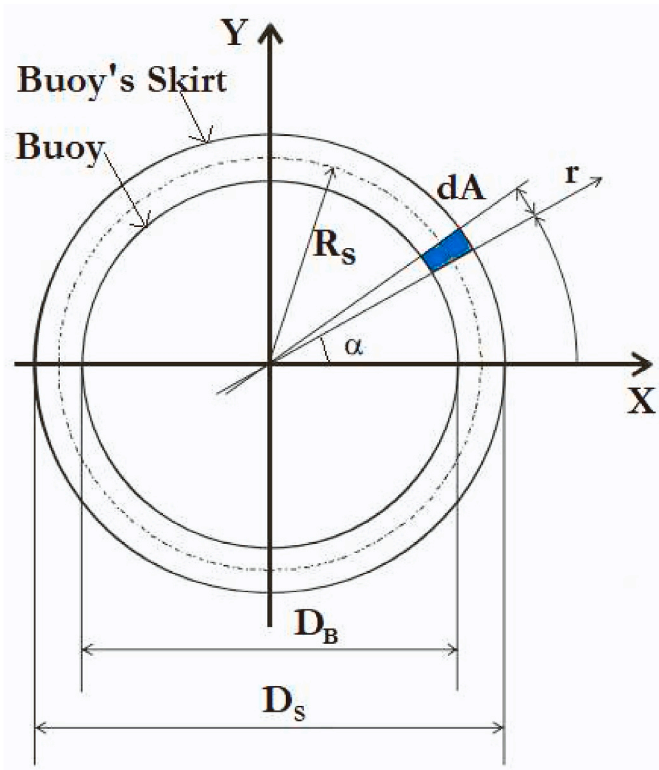

Fig. 18. Diagram describing the CALM Buoy Geometry and the Skirt Dimension for Cylindrical Buoy (CB).

4.1. Results of buoy motion from buoy geometry and skirt dimensions

4.1.1. Effect of geometrical shape and skirt size on buoy's motion

The skirts on the buoy presented in Table 11 and Figs. 18–19 were investigated for effect in this sub-section. Two geometries were considered-cylindrical buoy (CB) and square buoy (SB). As shown in Fig. 19(a–c) and 21(a-b), *BuoySkirt1* (13.90m diameter) had the least surge RAO while *BuoySkirt3* (11.90m diameter) had the highest surge RAO for the CB cases. Thus, the higher the skirt diameter, the lesser the surge RAO. Fig. 21(b) shows that *BuoySkirt1* has maximum surge RAO at 215,191 N/(m/s). Thus, the diameter of the buoy skirt affects the radiation damping. As shown in Fig. 19(d–f) and 21(c-d), *BuoySkirt1* (13.90m diameter) had the least surge RAO while *BuoySkirt3* (11.90m diameter) had the highest surge RAO for the SB cases. Thus, the higher the skirt diameter, the lesser the surge RAO. Fig. 21(d) shows that *BuoySkirt1* has maximum radiation damping at 315,239 N/(m/s). Thus, the length of the buoy skirt affects the radiation damping. In addition, the geometry affects the radiation damping, as the square buoy (SB) was higher than that of the cylindrical buoy (CB). The SB also had higher surge RAO than the cylindrical buoy, as such when model, it would be recommended to have some floats around the SB design to reduce the vortex effect around it, and to reduce it damping. A CFD is recommended to confirm this physics on the vortex flow field around the buoy. The results showed the effect of the buoy skirts on the motion RAOs and radiation damping, as other hydrodynamic properties will be discussed in subsequent sections.

4.1.2. Effect of geometry and skirt on response amplitude operators (RAO)

The RAOs were investigated on the dominant response recorded in the surge DoF (degrees of freedom) and heave DoF at 0° wave orientation. The same water depth was used for the different environmental conditions. In this study, the effect of skirt on the RAO of free-floating CALM buoys of two different geometries, and skirt dimensions is investigated. As recorded on Fig. 22, the surge RAO of the square buoy (SB) was higher than that of the cylindrical buoy (CB). The pattern was also seen to be similar but the higher the skirt diameter and skirt length, the higher the surge RAO. However, as recorded on Fig. 23, the heave RAO of the square buoy (SB) was lower than that of the cylindrical buoy (CB). The less the skirt diameter and skirt length, the higher the heave RAO. The *CB* BuoySkirt1@11.90m experienced the highest heave RAO while the *CB* BuoySkirt1@13.90m has the highest surge RAO. As such, it can be reported that it is pertinent to balance the CALM buoy due to these amplitudes by considering the natural periods, both in its hydrostatics/stability and hydrodynamics analysis. In a similar study (Boo and Shelley, 2021), a mooring buoy was designed for a WEC platform by considering the two buoy geometrical designs as well as the mooring

Table 12
Parameters for buoy hydrostatics.

Parameters	Value
Centre of Gravity (m)	−2.2
Buoyancy Force (N)	1,967,500
Area (m^2)	438.49
Volume (m^3)	344.98
Moment of Inertia, I_{xx} ($Kg.m^2$)	4,331,379.37
Moment of Inertia, I_{yy} ($Kg.m^2$)	4,486,674.11
Moment of Inertia, I_{zz} ($Kg.m^2$)	4,331,379.37

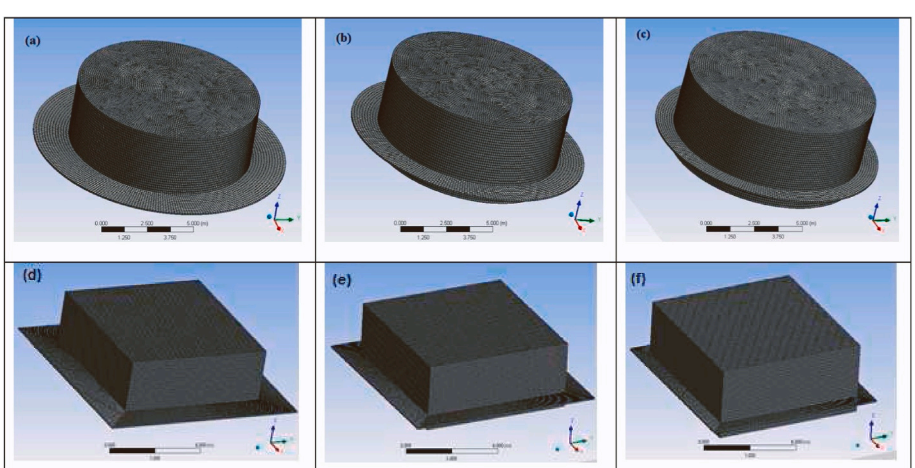

Fig. 19. CALM buoy of skirt diameter, for Cylindrical Buoy (CB) and Square Buoy (SB) Geometries, showing (a) $Ds_{1.CB}$ = 13.90m, (b) $Ds_{2.CB}$ = 12.90m, (c) $Ds_{3.CB}$ = 11.90m, (d) $Ds_{1.SB}$ = 13.90m, (e) $Ds_{2.SB}$ = 12.90m and (f) $Ds_{3.SB}$ = 11.90m.

Table 13
Hydrostatic stiffness matrix of buoy (in N/m, N and N-m).

Mode	Surge, X	Sway, Y	Heave, Z	Roll, RX	Pitch, RY	Yaw, RZ
Surge, X	0	0	0	0	0	0
Sway, Y	0	0	0	0	0	0
Heave, Z	0	0	789400	−0.06572	0.26092	0
Roll, RX	0	0	−0.06572	6882700	0.78336	−0.088372
Pitch, RY	0	0	0.26092	0.78336	6882700	−0.016425
Yaw, RZ	0	0	0	0	0	0

Table 14
Added mass matrix for the buoy.

Mode	Surge, X	Sway, Y	Heave, Z	Roll, RX	Pitch, RY	Yaw, RZ
Surge, X	26.641	0	0	0	104.79	0
Sway, Y	0	26.641	0	−104.79	0	0
Heave, Z	0	0	500.92	0	0	0
Roll, RX	0	−104.79	0	3930	0	0
Pitch, RY	104.79	0	0	0	3930	0
Yaw, RZ	0	0	0	0	0	1.29E-9

Table 15
Damping matrix for the buoy.

Mode	Surge, X	Sway, Y	Heave, Z	Roll, RX	Pitch, RY	Yaw, RZ
Surge, X	7.3229	0	0	0	16.732	0
Sway, Y	0	7.3229	0	−16.732	0	0
Heave, Z	0	0	0.0252	0	0	0
Roll, RX	0	−16.732	0	3930	0	0
Pitch, RY	16.732	0	0	0	32.7	0
Yaw, RZ	0	0	0	0	0	178E-12

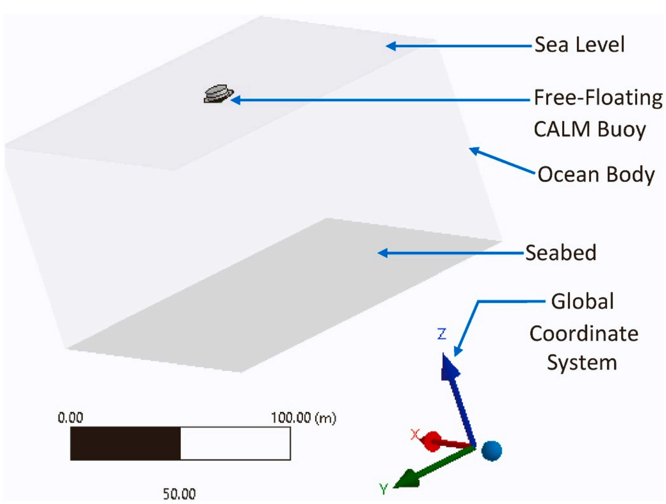

Fig. 20. Model Ocean View showing the free-floating CALM Buoy in ANSYS AQWA R2 2020.

tensions, and observed that the size of the buoy effects its motion RAOs. In conclusion, the motion RAOs are very important in the design of CALM buoys with skirt. The performance of the CALM buoy with skirt from this research shows that with an increase in the diameter of the skirt, that the surge and the heave motions will be increased.

4.1.3. Effect of geometry and skirt on radiation damping

The Radiation Damping was investigated on the dominant response recorded in the surge DoF and heave DoF at 0° wave orientation. The same water depth was used for the different environmental conditions. In this study, we have looked at the effect of skirts on the radiation damping of free-floating CALM buoys of two different buoy geometries and skirt dimensions. As recorded in Fig. 24, the surge radiation damping of the square buoy (SB) was higher than that of the cylindrical buoy (CB). The pattern was also similar but the higher the skirt diameter and skirt length, the higher the surge radiation damping. However, as observed on Fig. 25, the heave radiation damping of the cylindrical buoy (CB) was higher than that of the square buoy (SB) per skirt size. The higher the skirt diameter and skirt length, the higher the heave radiation damping. The CB BuoySkirt1@13.90m experienced the highest heave radiation damping for the cylindrical buoy, while the *CB* BuoySkirt1@11.90m has the lowest surge radiation damping. For the square buoy, the *SB* BuoySkirt1@13.90m experienced the highest heave radiation damping while the *SB* BuoySkirt1@11.90m has the lowest surge radiation damping. Thus, the radiation damping has some influence on the hydrodynamics of the CALM buoy. In principle, the damping coefficients in heave will be decreased with an increase in the skirt diameter, and thus the damping coefficients in heave will be decreased. As such, further investigation on the viscous damping of the CALM buoy is recommended. It is noteworthy to add that from this investigation, the thin skirt has an influence on the buoy's radiation damping in surge direction although this was expected mainly in heave, roll and pitch but not surge (Cozijn et al., 2005). As such, it is recommended that the design of CALM buoy should also include the surge damping, because there is radiated waves from the skirt that could affect the motion behaviour of the CALM buoy with skirt. However, it is subject to further comparison for buoys with and without skirts.

4.1.4. Effect of geometry and skirt on added Mass(es)

The influence of added mass(es) along the submerged part of the CALM buoy were studied at 0° flow angle, and for irregular wave with results as presented in Fig. 26(a–d) and 27(a-f). At 0° flow angle, the CALM buoy formation happens to be symmetrically oriented along X and Y directions, for the square buoy (SB) and cylindrical buoy (CB). Thus, the total surface area is the same, which creates similar hydrodynamic behaviour in the sway and surge directions. As can be observed, the square buoy (SB) showed higher sway added mass and surge added mass than the cylindrical buoy (CB). For the yaw added mass, it has very close correlation for the three skirt dimensions in both the square buoy (SB) cases in Fig. 26(c) and the cylindrical buoy (CB) cases in Fig. 26(d). However, it can be observed that the higher the skirt size, the lesser the yaw profile in SB cases, but it is slightly almost the same in CB cases, except where the profile peaks and troughs, as observed in Fig. 26(c). For the pitch added mass in Fig. 30, each buoy size had a unique similar relationship. *SB* BuoySkirt1@13.90m in Fig. 27 (a) was similar to *CB* BuoySkirt1@13.90m in Fig. 27(b), and same for other buoy sizes. It can be observed that an increase in the buoy skirt size also increases the added mass, and this is expected. However, increasing the frequency of the wave will decrease this response characteristics gradually. Therefore, it can be opined that the added mass components for the rotational sections of the sway and surge motions. They are almost 3 times lower than the masses of their corresponding translational sections. The performance of the CALM buoy with skirt shows that with an increase in the diameter of the skirt, that the added mass in

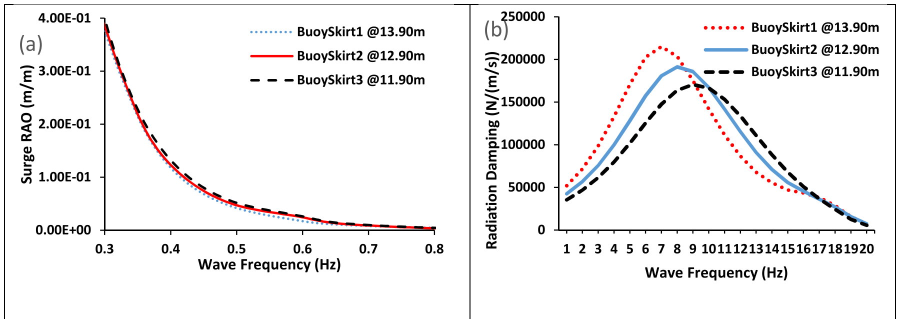

(a) Buoy skirt diameters of CB on Surge RAO (b) Buoy skirt diameters of CB on Radiation Damping

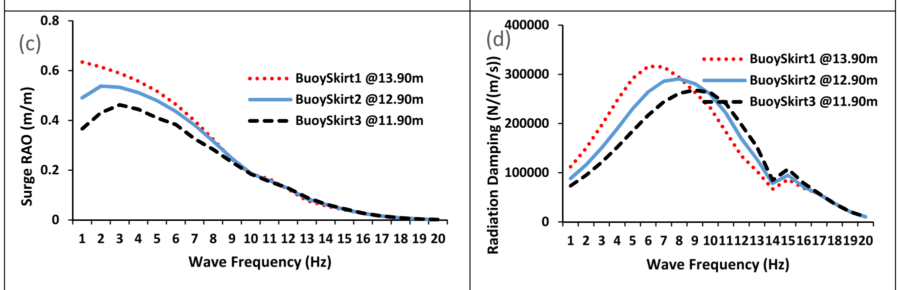

(c) Buoy skirt diameters of SB on Surge RAO (d) Buoy skirt diameters of SB on Radiation Damping

Fig. 21. Effect of buoy skirt diameters of Cylindrical buoy.

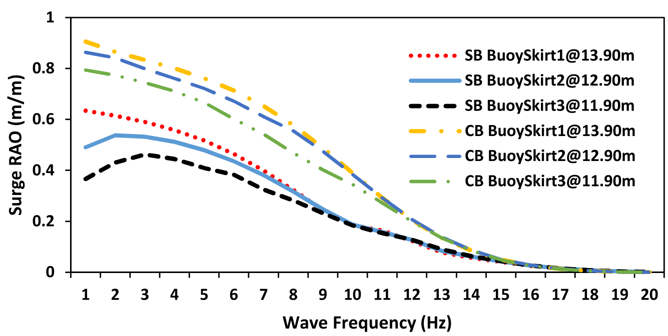

Fig. 22. Surge RAO for Square Buoy (SB) and Cylindrical Buoy (CB) for free floating case.

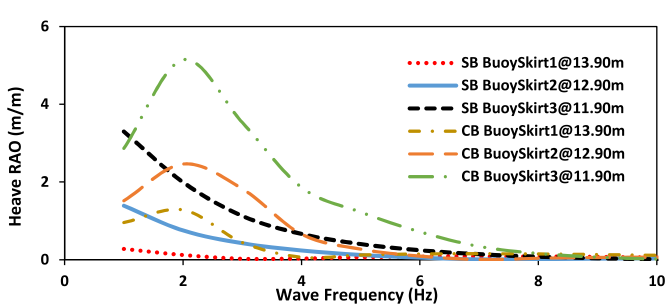

Fig. 23. Heave RAO for Square Buoy (SB) and Cylindrical Buoy (CB) for free floating case.

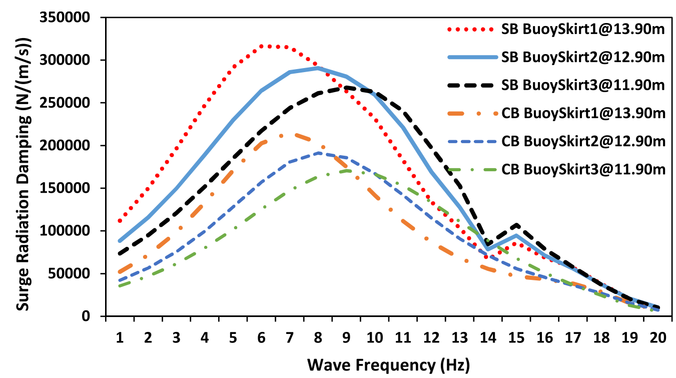

Fig. 24. Surge Radiation Damping for Square Buoy (SB) and Cylindrical Buoy (CB) for free floating case.

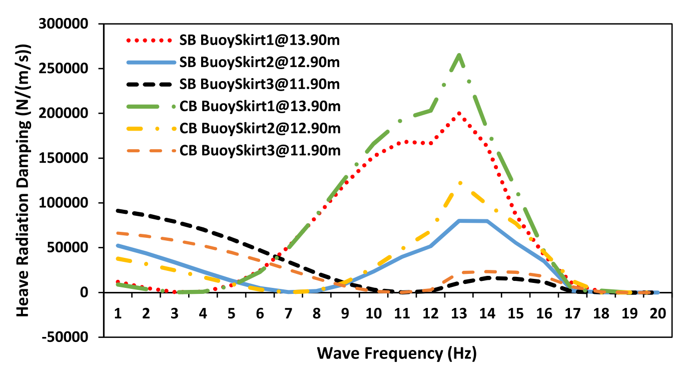

Fig. 25. Heave Radiation Damping for Square Buoy (SB) and Cylindrical Buoy (CB) for free floating case.

pitch and the added mass in heave will be increased.

4.1.5. Effect of geometry and skirt on wave exciting force

The effect of the influence of wave exciting force along the submerged part of the cylindrical CALM buoy were studied at 0° flow angle, and for irregular wave with results as presented in Fig. 28(a–f). It is observed that the buoy skirts have an influence on the amplitudes of the wave exciting forces on the 6DoFs, especially the heave exciting force and the pitch exciting force. Thus, there will be need to dampen the buoy by increasing the added mass or increasing the coefficient of damping, C_d used.

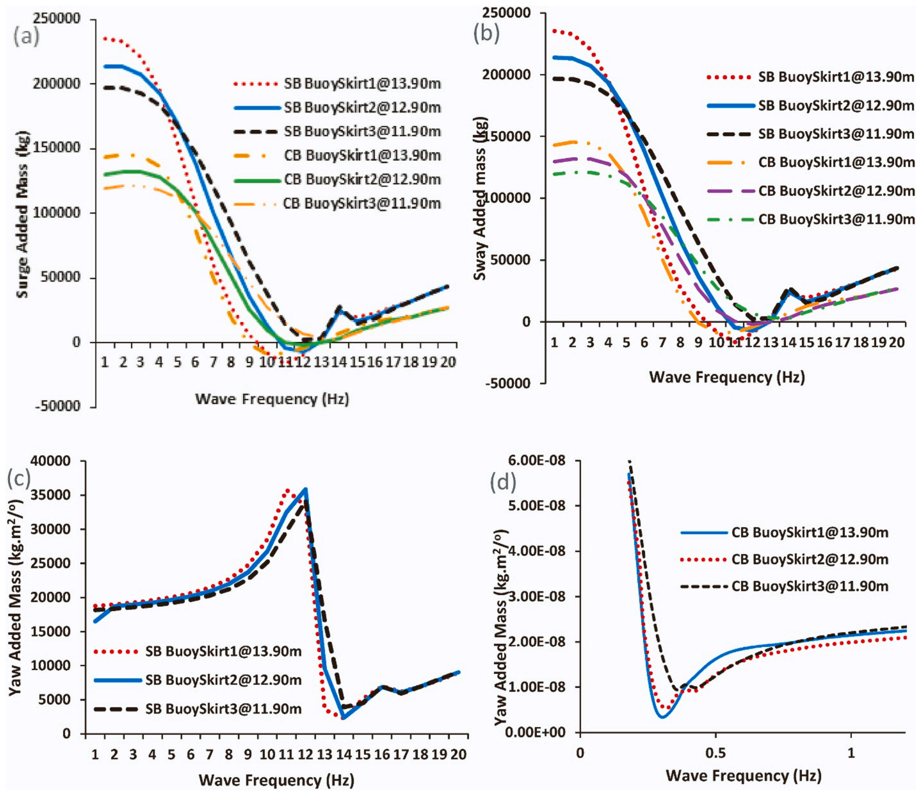

Fig. 26. Surge, Sway, and Yaw Added Mass for Square Buoy (SB) and Cylindrical Buoy (CB), where (a) Surge, (b) Sway, and (c) SB Yaw and (d) CB Yaw added masses for free floating case.

4.1.6. Effect of buoy position and acceleration response

The results of the effect of buoy response for the actual position carried out on the CALM buoy in ANSYS AQWA, using the Square Buoy (SB) is presented in Fig. 29. It was investigated using the environmental data for Case1 in Table 7 and the oceanic data in Table 11. It was observed that the surge acceleration of the buoy was least acceleration of 5.45 x 10^{-7} m/s^2 in *BuoySkirt1* which has a diameter of 13.90m, while the smallest skirt *(BuoySkirt3)* had the highest surge acceleration of 9.233 x 10^{-7} m/s^2 as seen in Fig. 29(a). This means that the bigger the skirt diameter, the less the surge acceleration on the buoy. From Fig. 29 (d), the heave acceleration shows that the skirt size had no noticeable effect as they all had the same heave acceleration with a linear relationship as in Equation (16), as $\boldsymbol{y = -0.07x -2.2}$, with an $\boldsymbol{R^2 = 1}$. It is noticed that the acceleration is very small, based on the low frequency used in the diffraction study. Secondly, the position and acceleration response of a CALM buoy is much smaller, in comparison with bigger structures like tension leg platforms (TLPs), floating offshore wind turbine (FOWT) and floating semisubmersibles (Mohamed, 2011; Odijie, 2016, Kashiwagi M. 2000, Pham and Shin, 2019).

$$y = -0.07x - 2.2,\ R^2 = 1 \tag{16}$$

4.2. Results of wave-current interaction based on buoy motion

4.2.1. Effect of incident angle on buoy's pressure and motion characteristics

The effect of incident angle on the pressure and motion of the CALM buoy was carried out in ANSYS AQWA. It was observed that an increase in the incident angle amplitude, $\boldsymbol{a}$ increased the wave frequency, $\boldsymbol{f}$ for the wave angles investigated, as shown in Figs. 30–31. By definition, the incident angle can be stated to be the angle which the waves make with the body of the buoy, and it has an effect on the motion response of the CALM buoy. In Fig. 30(a and b), the highest incident angle recorded the highest wave frequency at an amplitude of 2.5m. Fig. 30(b) gives a plot with a linear relationship as in Equation (17), as $\boldsymbol{y = -0.702x -0.0014}$, with an $\boldsymbol{R^2 = 1}$. This shows that there is linearity in the parameters for the same wave heading. From the pressure and motions analysis, it can be observed that different flow angles have varying effects on the CALM buoy. Using a structure interpolated pressure contours with pressure measured at the head of water, the contours in Fig. 30 were generated. Fig. 30(a–e) shows profiles of pressure and motions contour plots for Cylindrical Buoy (CB) under different wave amplitudes from 0.5m to 2.5m at an incident angle of 180°. Fig. 30(f) presents the pressure and motion on CALM buoy at an incident angle of 30°, conducted in ANSYS AQWA. It shows the effect of flow angle for the wave heading on the buoy's hydrodynamics. As the incident angle is from wave heading, there will be an increase in the harshness effect of the waves on the CALM buoy. The hull deformation, $\boldsymbol{\delta}$ increases with wave amplitude, $\boldsymbol{a}$ as seen in Figs. 30–31. Thus, the higher the wave amplitude, the higher the deformation. This phenomenon of accessing the deformation from motion behaviour is quite related to mechanics of statics whereby the buoy's stiffness is a function of the deformation under these loading effects. The study of the pressure and motion is important as it can be used to predict the motion behaviour and load transfer mode in the design of the CALM buoy. Earlier studies showed that some wave energy are absorbed also when waves hit bodies, but they differ for elongated bodies, deformable bodies and rigid bodies (Newman, 1979, 1994; Bishop and Price, 2005). As the incident angle increases, the wave amplitude increases and also the wave frequency, which will lead to higher deformation on the buoy body from the waves, however, the impact of water waves may not be detrimental, but it may have some deformation on the body. Similar behaviour in slender bodies are related to some wave damping terms in the system (Aranha and Martins, 1997). Thus, the buoy designer will need to design the buoy by considering vortex effect reduction, such as with strakes, customised pneumatic fenders or other coupling approaches numerically. Based on coupled modelling approach (Cozijn et al., 2004; Bunnik et al., 2002; Gu, 2016; Gu et al., 2017, 2019), further work could include CFD study on the

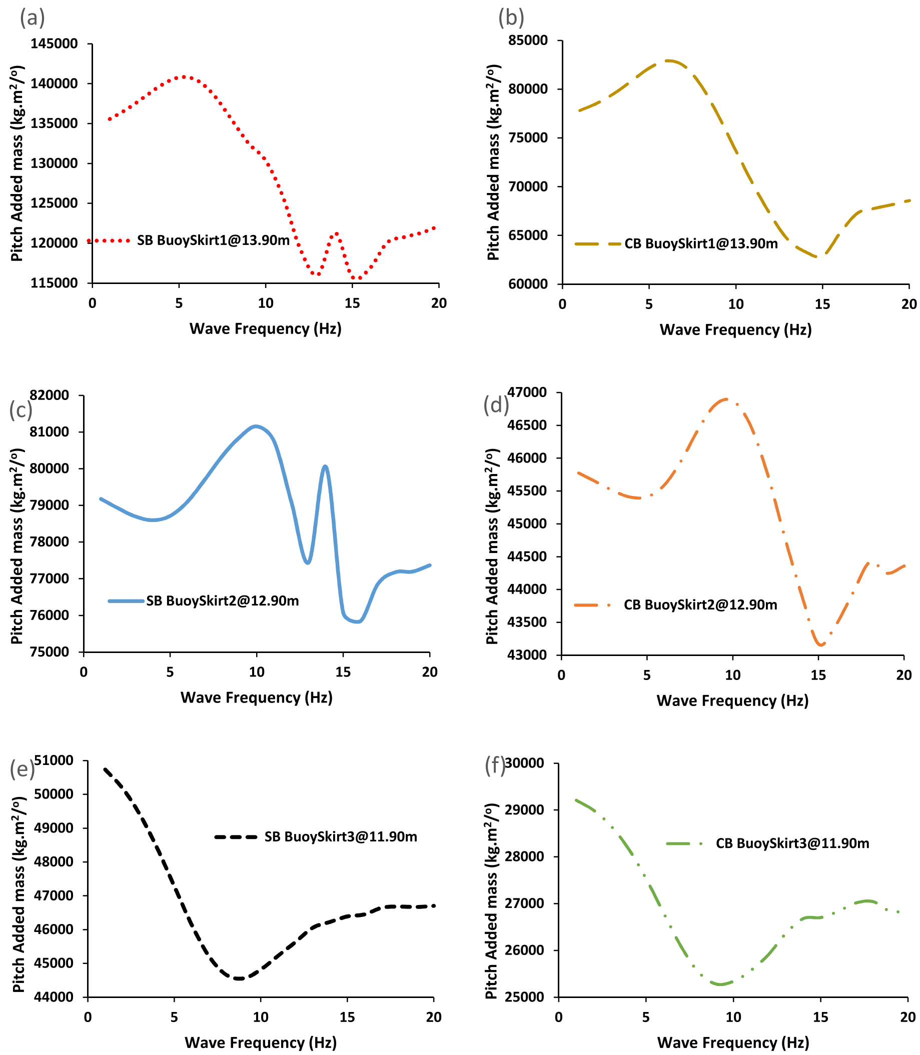

Fig. 27. Pitch/Roll Added Mass for Square Buoy (SB) and Cylindrical Buoy (CB), where (a) SB BuoySkirt1@13.90m Pitch, (b) CB BuoySkirt1@13.90m Pitch, (c) SB BuoySkirt2@12.90m Pitch, (d) CB BuoySkirt2@12.90m Pitch, (e) SB BuoySkirt3@11.90m Pitch and (f) CB BuoySkirt3@11.90m Pitch for free floating case.

reduction of damping and vortex effect, such as using Q-criterion to observe the vorticity around the CALM buoy.

$$y = -0.702x - 0.0014, \; R^2 = 1 \tag{17}$$

4.2.2. *Effect of wave headings on buoy hull deformation*

The effect of CALM buoy hull deformations were investigated using different wave headings. Figs. 32 and 33 present the deformation on the Cylindrical CALM Buoy (CB) under different wave headings at 1m amplitude. As the wave headings increases in phases, the deformation decreases from 0° and at 60°, it increases to 90° and then decreases up to at 120° before increasing again to 150°. This deformation plot presents a sinusoidal formulation which is relative to both the water waves and water depth. In this present study, the wave heading had a maximum deformation at the flow incidence between 30° and 60°. This was noticed from the RAO plots to result from the reduced motions experienced by the buoy's hull across this flow angle range. The sections of the buoy's body that are buried below the wake of the flow from the wave heading experience more significant deformations due to drags that developed around the body, or near the skirt. Since it is a cylindrical buoy, drag development would require sharp vertices at certain angles or flow orientations. As presented in Section 1.0, drag is a vital component of the Morison's equation (Morison et al., 1950). Thus, it would be pertinent that additional loading analysis on the wave amplitude and wave-current interaction is conducted, as presented herein. More studies were carried out on the pressure and motion of the CALM buoy operated in ANSYS AQWA to investigate the extent of hydrostatic and hydrodynamic loadings from the waves. There is presently no publication found on this study for CALM buoys, thus the novelty here. Similar studies have been conducted on semisubmersibles like PCSemi (Zou et al., 2013; Odijie and Ye, 2015b). In the former study (Zou et al., 2013), a contrast on the influence of current headings from motion responses were presented. In the later study (Odijie and Ye, 2015b), the effect of the wave headings on the hull of the PCSemi was studied for an understanding of its fluid-structure interaction (FSI) using FEM. However, it is recommended to further investigate this behaviour under varying water depths.

4.2.3. *Effect of CALM buoy motion on Hose's bending moment and effective tension*

The effect of CALM buoy motion on attached marine hose was also investigated in this section, to assess the bending moment and effective tension along the hose-string. The hose profile used is represented in the Lazy-S submarine hose in a recent marine hose study (Amaechi et al., 2021e). It has been observed that the buoy motion also has some mechanical influence on the bending moment and effective tension of the submarine hoses and floating hoses. Fig. 34(a) is the result of bending moment for 3 environmental cases *(Case1, Case2 and Case3)* as presented in Table 7, while Fig. 34(b) is the effective tension. High bending

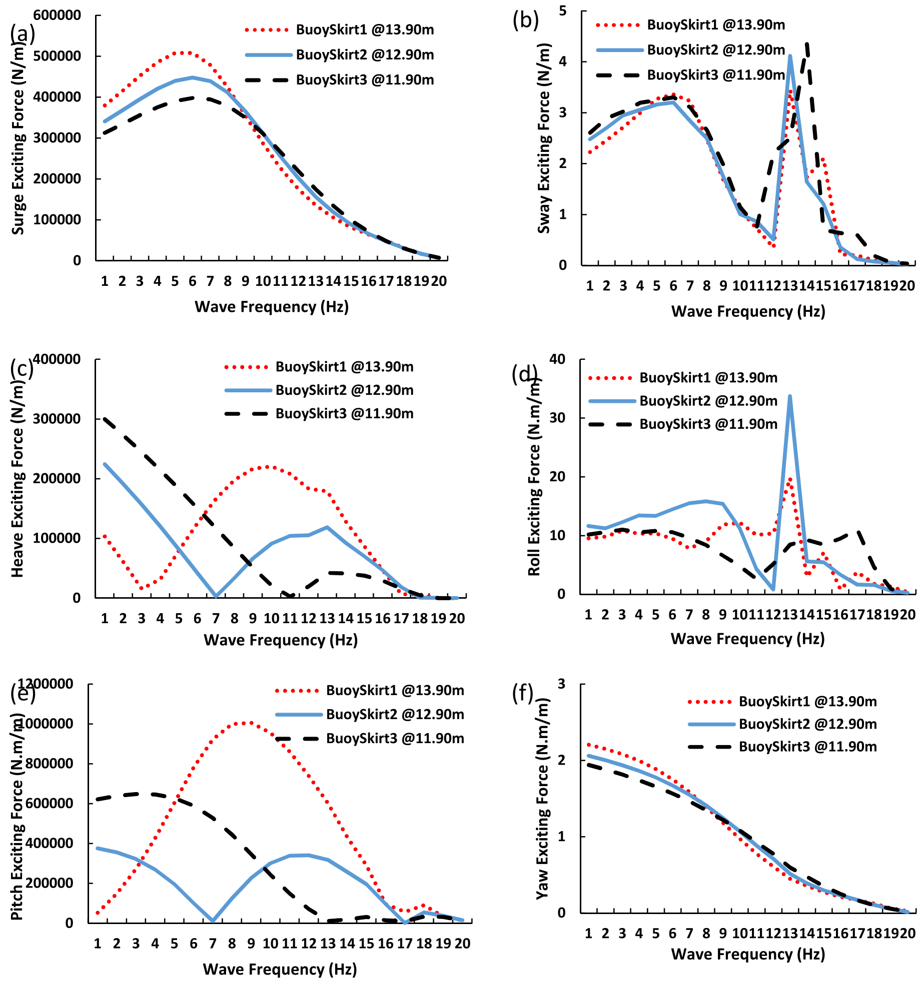

Fig. 28. Wave exciting force for the 3 buoy skirt sizes for the Cylindrical Buoy (CB), where (a) surge, (b) sway, (c) heave, (d) roll, (e) pitch and (f) yaw.

moment of the submarine hose was noticed around the connections, as such, it is recommended that such locations be highly reinforced. Also, the higher the significant wave height, the lesser the bending moment, as *Case 3 bending moment* is lower than *Case 1 bending moment*. In Fig. 34 (b), it can be observed that there is high effective tension at the top connection of the submarine hose to the CALM buoy of 106.24 kN. It is important to include the attachments to the CALM buoy in the study because high bending moment can induce some load on the RAO generated by the CALM buoy. RAO, like other hydrodynamic properties, have an influence on the behaviour of the CALM buoy hose system, and particularly long the submarine hose length. However, it is also influenced by the buoy motion. There was relatively higher level of effective tensions observed at the top end of the hose, as seen in Fig. 34(b), which are significantly higher than those along other parts of the arc length in-between. The CALM buoy has an effect on the tension of the hose-string, as this top end has highest axial and flexural stiffness due to the end-restrictions, compared to other relatively flexible sections of the hose-string. It is recommended to consider the use of more flexible hose sections with less bending moments to withstand the hydrodynamic loads. For the bending moment of the three cases investigated, there is significantly higher bending moments observed at both ends than those in-between, as the hose has higher flexural stiffness at both the top connection and the touch down point area. This can be due to the twisting behaviour of the hose end connecting the CALM buoy, or the bending stiffness of that section of the hose-string. When it is compared to its initial hose position, the twisted hose may be challenged with fluids since contact exists between the moving content and the internal surface of the hose at locations. This can lead to hose bending-fatigue, significant twisting deformations, and twisting in relation to the wave angles. As the hose twists, the bending moment changes along the arc length of the hose. As such, it is recommended to carry out a bending-fatigue assessment on hoses. This is recommended in further study.

4.2.4. Effect of current on CALM buoy motion and waves-current interaction

The influence of currents on the waves-current interaction was investigated on the CALM buoy, by using the environmental conditions for Case1 as given in Table 6. The values for the zero-up-crossing period Tz, the significant heights Hs, and the peak period Tp are 4.10s, 1.87m, 5.27s, respectively. The following values were kept constant for all the runs used: the waves direction is 180°, the seabed current speed is 0.45 m/s, the current direction is 180°, the wind speed is 22 m/s, and the wind direction is 0°. Using JONSWAP wave spectrum with these same values, the surface current and waves interactions were studied. The value varied for the surface current in this waves-current interaction study are: 0.5 m/s, 0.75 m/s, 1.0 m/s, 1.25 m/s and 1.5 m/s. Studies on waves-current have been conducted on floating structures like semi-submersibles (Odijie, 2016; Mohamed, 2011) and offshore wind turbines (Chen and Basu, 2018). Thus, there is also novelty in this present study based on wave-current interaction for CALM buoys, making this study crucial, as there is limited literature in this subject area. As observed on Fig. 35(a–f), the current velocity increases with increase in frequency for the spectral densities of the 6DoFs. Hence, this shows good

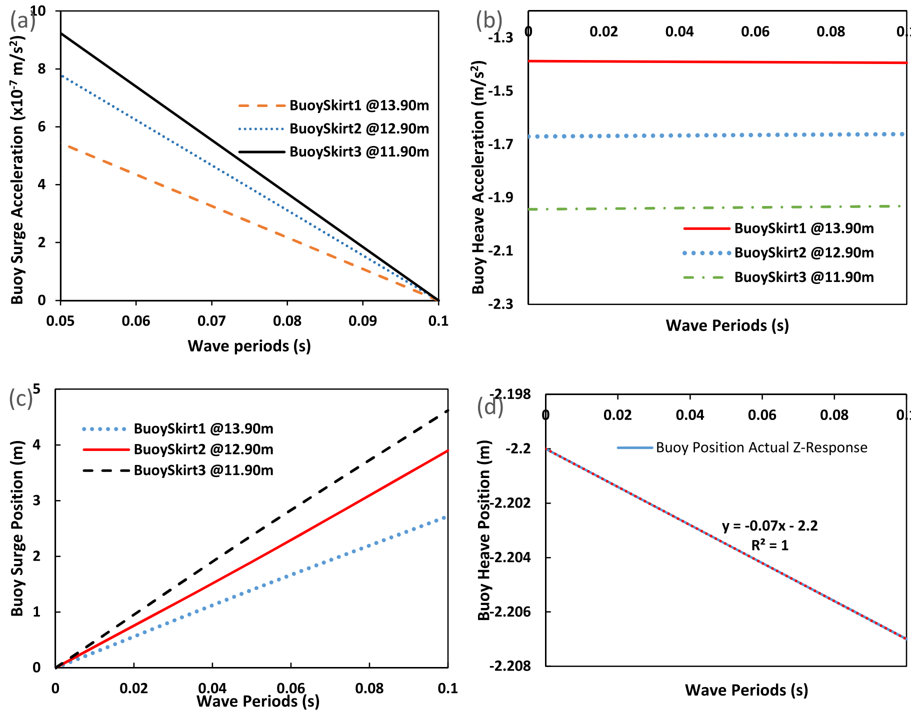

Fig. 29. Square Buoy (SB) time response showing (a)structure acceleration actual response, (b) heave acceleration actual response, (c) Surge position actual response and (d) Heave position actual response.

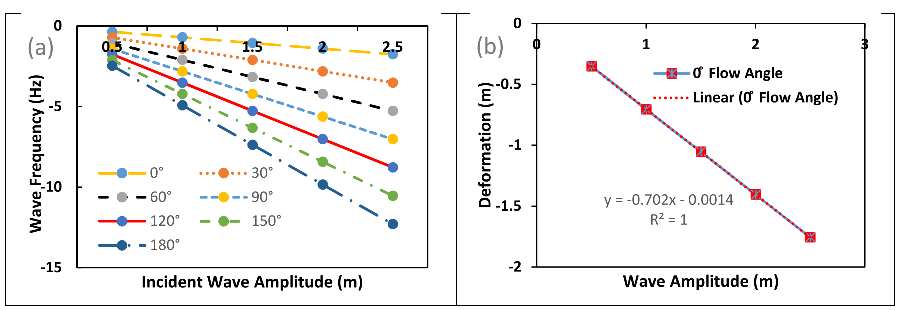

Fig. 30. The CALM buoy study showing (a) Incident angle on Pressure and Motion of the buoy, and (b) Buoy wave amplitude on Pressure and Motion of the buoy hull.

behaviour from the waves-current interaction as expected.

4.2.5. Effect of seabed model on CALM buoy motion and waves-current interaction

The influence of seabed models on waves-current interaction was investigated on the CALM buoy. The numerical model was developed for irregular waves on the CALM buoy system in 100m water depth on the same non-linear seabed. Table 8 gives the parameters for the linear seabed while Table 16 gives the parameters for the non-linear seabed. Details of the nonlinear seabed model are available in the literature (Amaechi et al., 2021e; Orcina, 2014, 2021). For this assessment, the same current of 0.5 m/s was utilised in ocean environment. From Fig. 36 (a–f), it can be noticed that there are variations in the spectral densities of the two seabed models. For the translational motions, the linear seabed model has higher surge spectral density, sway spectral density and heave spectral density than the nonlinear seabed model. For the rotational motions, the nonlinear seabed model has higher roll spectral density, pitch spectral density and yaw spectral density than the nonlinear seabed model. This can be due to factors, such as the soil stiffness and its resistance. Thus, the current is also a good parameter in the assessment of soil models.

4.2.6. Effect of seabed profile, water depth and hose static offset on marine hose

The effect of water depth was conducted on the marine hoses configured using Lazy-S, as represented in Fig. 37(a and b). When comparing linear and nonlinear seabed models in Fig. 37(a), same behaviour was observed. As a result, it also verifies the suggested model's consistency. This profile, however, is not generic and is specific to this Lazy-S scenario, as each Lazy-S configuration will differ in terms of environmental loadings, hose buoyancy, water depth, buoyancy float location, and weight of the marine hose in water. The hose-string examination against the two seabed models (linear and nonlinear), reveals that the linear seabed model behaves differently from the nonlinear seabed model. The linear seabed model has a slightly higher configuration than the nonlinear seabed model as the water depth increases. This could be attributed to factors like repenetration, elevation, and soil resistance. Determining the highest soil shear stiffness that generates the least bending moment and the least effective tension under a (non)linear seabed model are instances for further research. Other aspects could include the impact of fluctuation or nonlinearity caused by seabed soil resistance, penetration rate, and uplift on the seabed. During static analysis, the influence of the hose layout was evaluated utilising a water

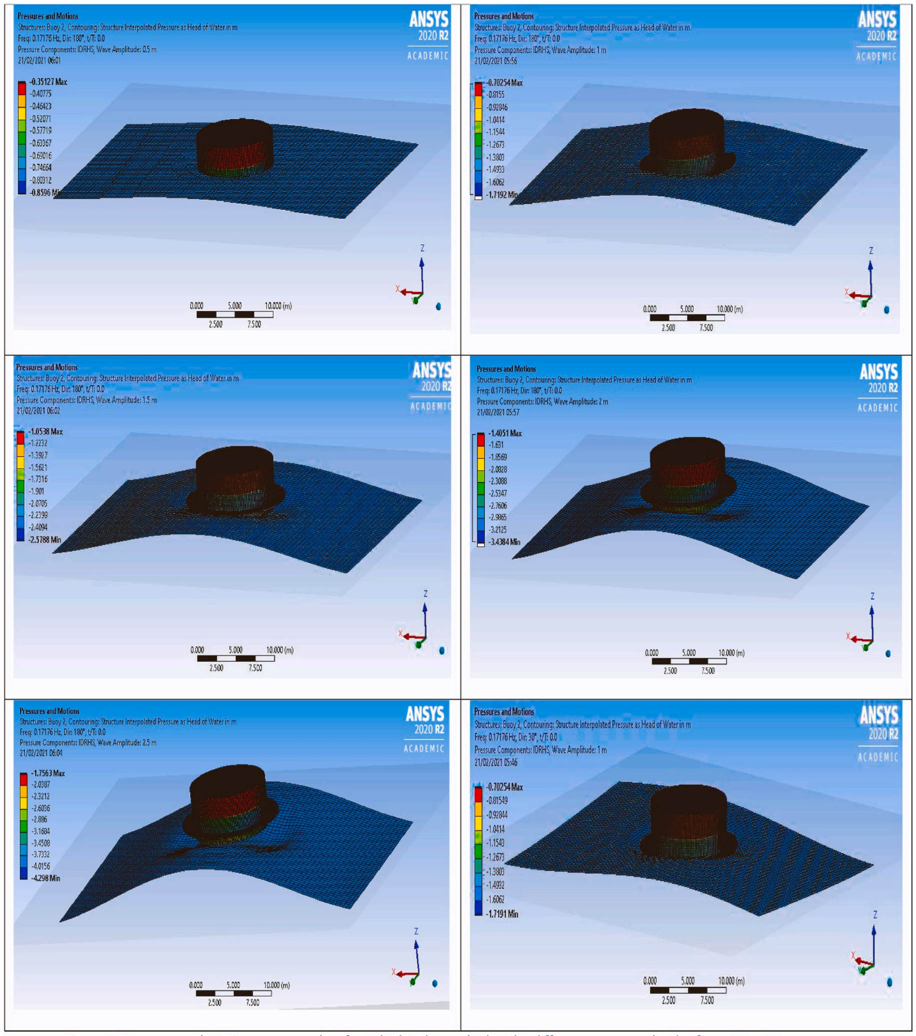

Fig. 31. Pressure and Motions contour plots for Cylindrical Buoy (CB) under different wave amplitudes from 0.5m to 2.5m, showing (a) 0.5m at 180°, (b) 1.0m at 180°, (c) 1.5m at 180°, (d) 2.0m at 180°, (e) 2.5m at 180° and (f) 1.0m at 30°.

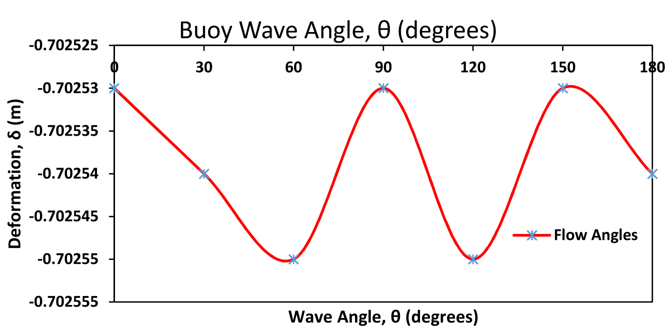

Fig. 32. Deformation on the Cylindrical CALM Buoy (CB) under different angles at 1m amplitude.

depth of 100m and a Lazy-S design. In the case of the static offset of the marine hose riser, the maximum values were higher than the minimum and mean values, as shown in Fig. 37(b). The plot shows consistency, and the maximum value is utilised in obtaining the extreme hose's static offset behaviour in the Lazy-S configuration. Due to the sheer buoyancy design, such as the usage of buoyancy floats, the hose-string takes the shape of a Lazy-S as the water depth deepens.

4.2.7. *Effect of surface current and seabed current on marine hose*

The influence of both the surface current and seabed current on the submarine hose was carried out. The surface current velocity plays an important role in the design of a loading and offloading CALM buoy system. To investigate its influence, some surface current values are used; for 0.45 m/s, 0.65 m/s, 0.75 m/s, 0.9 m/s and 1.0 m/s. As the surface current velocity increases, the bend radius (curvature) decreases, the bend moment decreases, and the effective tension increases, as in Fig. 37(a–d). Considering the seabed currents, the following seabed current velocities were considered: 0.35 m/s, 0.45 m/s, 0.75 m/s and 0.9 m/s. For the same surface current velocity, an increase in the seabed current velocity has a reduced effective tension and reduced bend moment, as shown in as in Fig. 38(e and f). An increase in seabed current velocity gives a reduced bend radius (Curvature), increased effective tension and bend moment.

4.2.8. *Effect of current velocity across water depth in WCI studies*

The effect of current velocity profile across water depth was investigated on the waves-current interaction (WCI) study. Fig. 39 shows the five (5) current range considered in the waves-current interaction study for the CALM buoy model in this sub-section with profiles across 0.5 m/s, 0.75 m/s, 1.0 m/s, 1.25 m/s and 1.5 m/s. It can be observed that the current profile used in the study is typical for a deepwater condition, where the current from −100m down to −200m remains almost

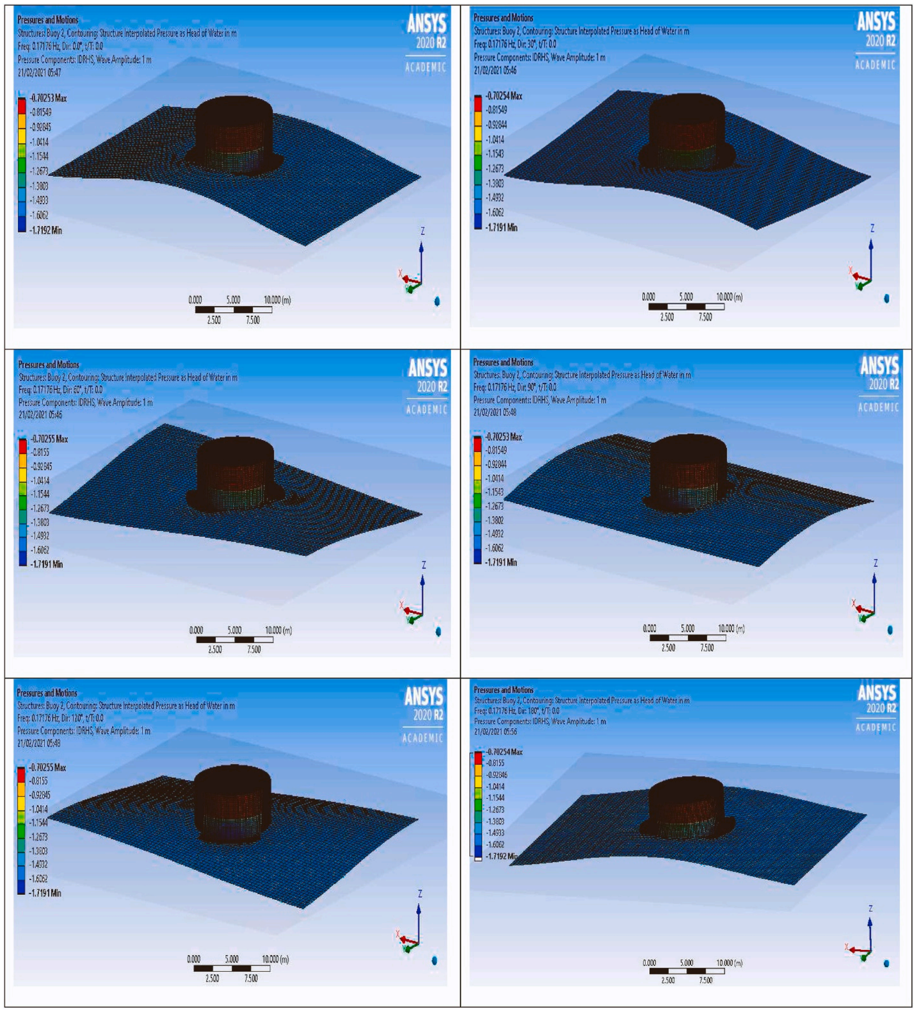

Fig. 33. Pressure and Motions contour plots for Cylindrical Buoy (CB) under different angles at 1m amplitude, for (a) 0°, (b) 30°, (c) 60°, (d) 90°, (e) 120° and (f)180°.

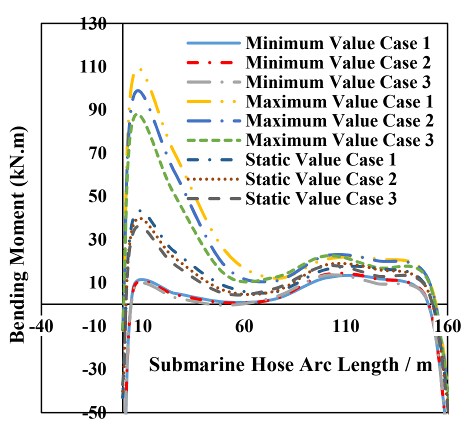

(a) **Bending moment of CALM buoy submarine hoses for 3 cases**

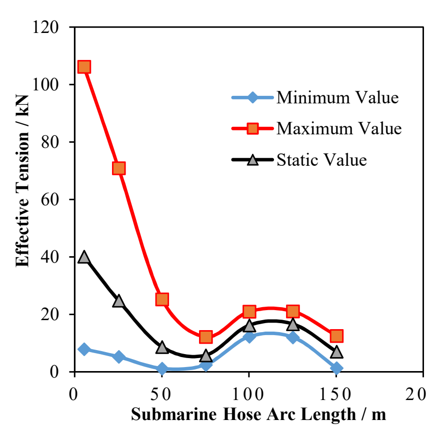

(b) **Effective Tension of CALM buoy submarine hoses for 3 cases**.

Fig. 34. Effect of CALM buoy motion on submarine hoses bending moment and effective tension.

constant. This shows that there are higher current velocity due to wind flows, tidal currents, waves effects and other radiation/diffraction forces on the top surface of the sea. In this study, there are different velocity profiles investigated at 0m, which are based on its effect on other parameters as discussed in earlier sections of this WCI study. The highest current velocity profile was noted to have highest response effect from this study as reported in Section 4.2.7. Thus, current is a key parameter for WCI investigation.

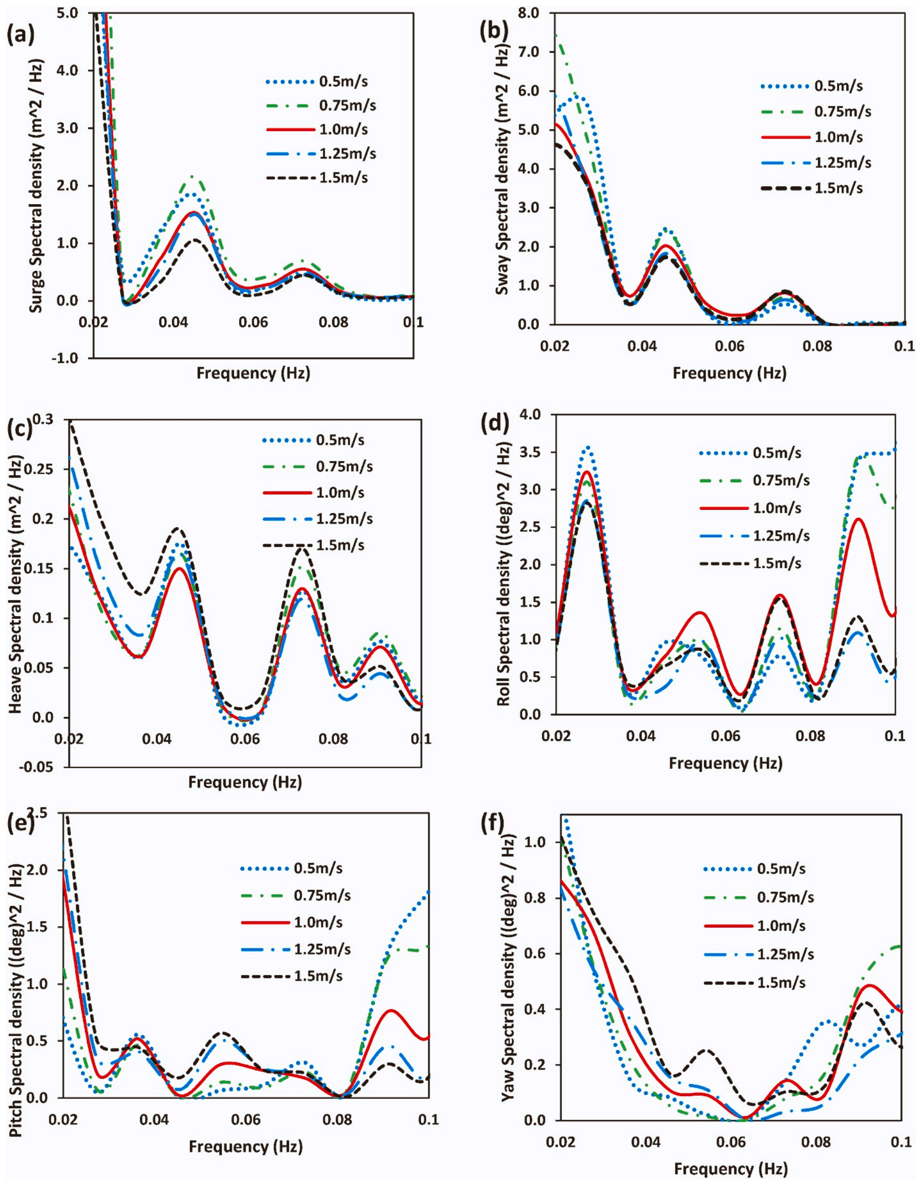

Fig. 35. Effect of current on CALM buoy motion showing spectral densities for: (a) surge, (b) sway, (c) heave, (d) roll, (e) pitch and (f) yaw.

Table 16
Non-linear soil model parameters.

Parameters	Value
Mudline Shear Strength, S_{u0} (kPa)	4.5
Shear Strength Gradient, S_g (kPa/m)	1.5
Saturated Soil Density, ρ_{soil} (te/m^3)	1.5
Power Law Parameter, a	6.0
Power Law Parameter, b	0.25
Soil Buoyancy Factor, f_b	1.5
Normalized Maximum Stiffness, K_{max} (kNm^{-1}m^2)	200.0
Suction Resistance Ratio, f_{suc}	0.7
Suction Decay Parameter, λ_{suc}	1.0
Repenetration Parameter, λ_{rep}	0.3

4.3. Discussion

The investigation on the motion characteristics of a CALM buoy has been successfully conducted in this study using two (2) buoys geometries and three (3) different skirt dimensions. These results in Sections 4.1-4.2 were based on the presented methodology presented in Section 3. However, from this study, the following observations and recommendations were made:

1. The higher the CALM buoy skirt diameter and skirt length, the higher the heave radiation damping. For the cylindrical buoy, the CB BuoySkirt1@13.90m experienced the highest heave radiation damping while the CB BuoySkirt1@11.90m has the lowest surge radiation damping. For the square buoy, the SB BuoySkirt1@13.90m experienced the highest heave radiation damping while the SB BuoySkirt1@11.90m has the lowest surge radiation damping. Thus, the radiation damping has a significant effect on the hydrodynamics of the CALM buoy. The buoy geometry also affected the radiation damping, as that of the square buoy (SB) was higher than that of the cylindrical buoy (CB). The SB model also had higher surge RAO than the CB model, as such when model. Reduction of damping will increase the motion, as seen in literature (Cozijn et al., 2005; Cozijn et al., 2004; Le Cunff et al., 2007). Therefore, an experiment on the motion behaviour of the CALM buoy is recommended to further validate these findings.

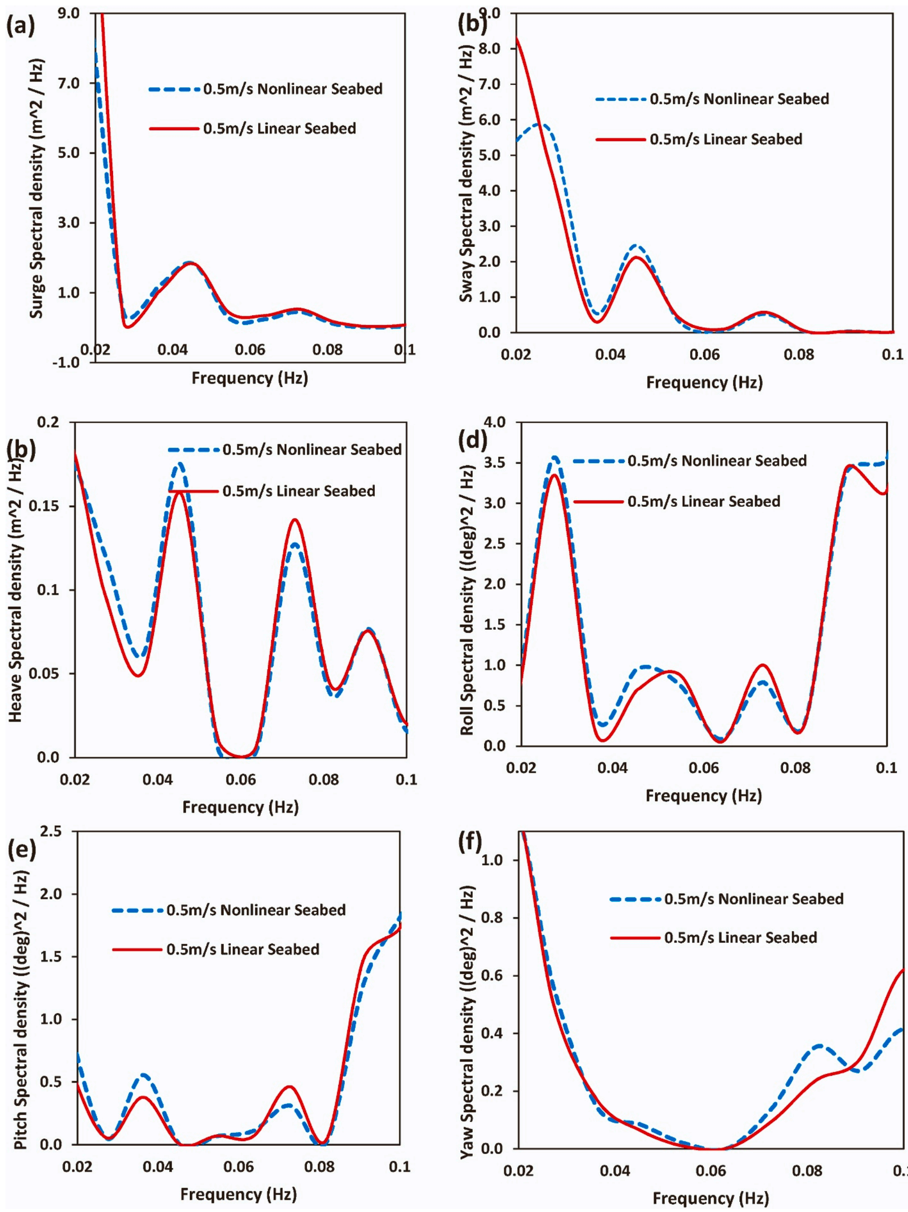

Fig. 36. Effect of seabed under current of 0.5 m/s for linear and nonlinear seabed models on the CALM buoy motion showing spectral densities for: (a) surge, (b) sway, (c) heave, (d) roll, (e) pitch and (f) yaw.

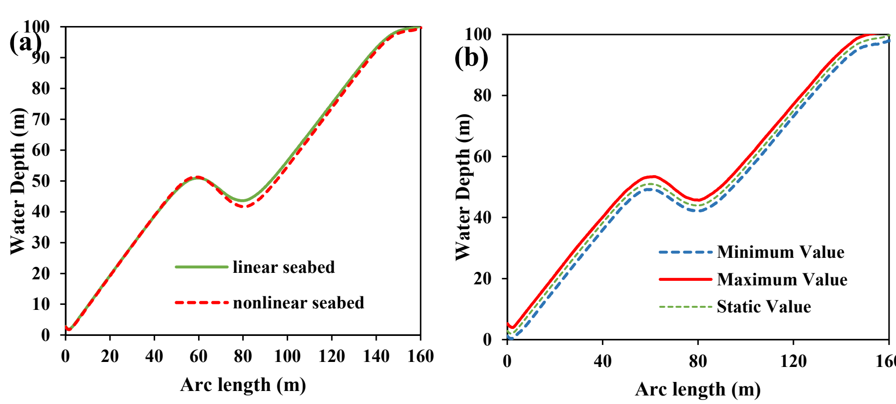

(a) Effect of water depth on static offset for linear and nonlinear seabeds.

(b) Effect of water depth on static offset configuration of lazy-S hoses for linear seabed.

Fig. 37. Effect of water depth and hose static offset on submarine hoses in Lazy-S configuration.

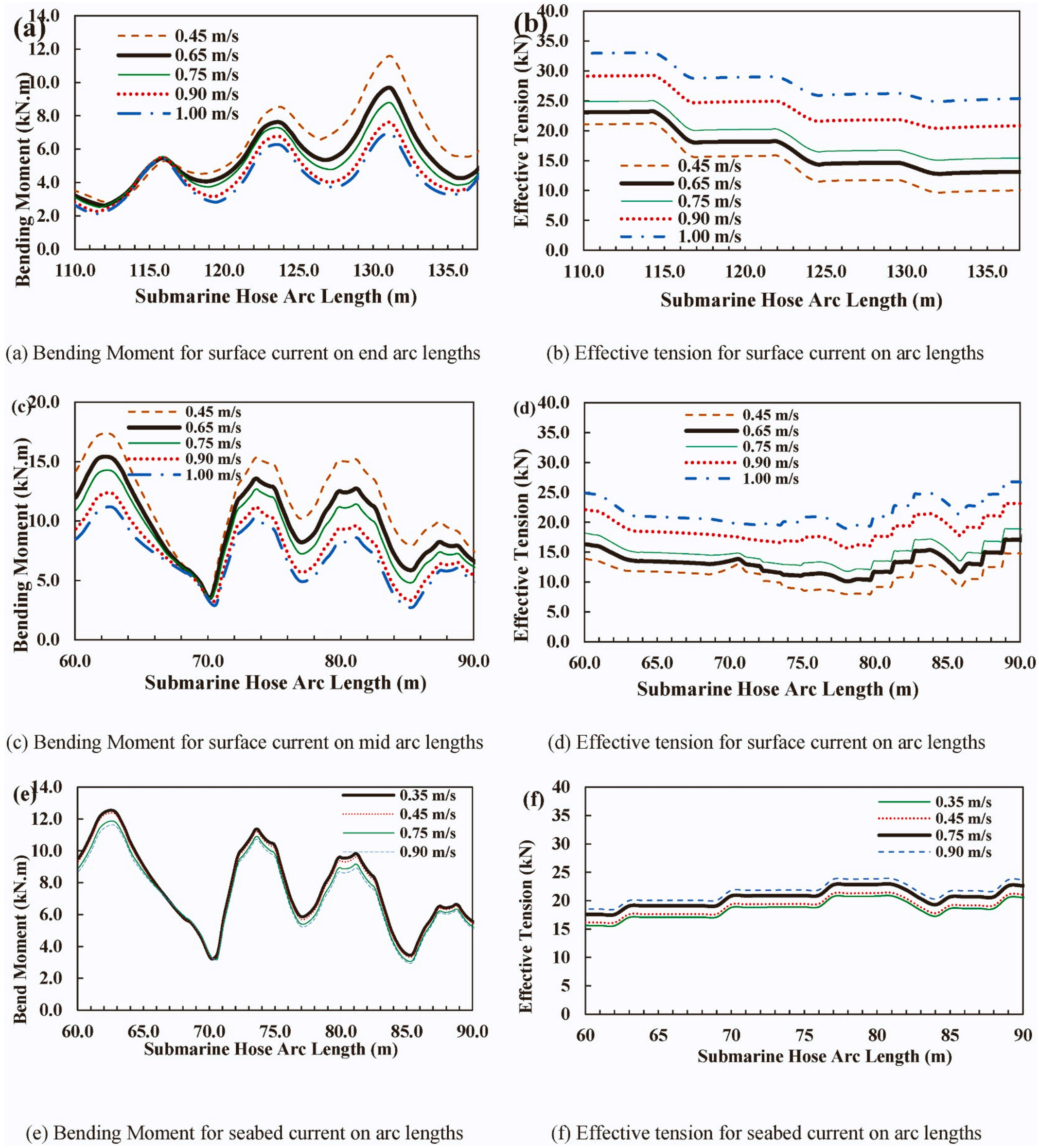

(a) Bending Moment for surface current on end arc lengths

(b) Effective tension for surface current on arc lengths

(c) Bending Moment for surface current on mid arc lengths

(d) Effective tension for surface current on arc lengths

(e) Bending Moment for seabed current on arc lengths

(f) Effective tension for seabed current on arc lengths

Fig. 38. Effect of surface currents (a–d) and seabed currents (e–f) on submarine hoses.

2. The surge RAO of the square buoy (SB) was observed to be higher than that of the cylindrical buoy (CB). The pattern was also seen to be similar but the higher the skirt diameter and skirt length, the higher the surge RAO. However, the heave RAO of the square buoy (SB) was lower than that of the cylindrical buoy (CB). The CB BuoySkirt1@11.90m experienced the highest heave RAO while the CB BuoySkirt1@13.90m has the highest surge RAO. As such, it can be seen that it is important to balance the stability of the CALM buoy due to these amplitudes by considering the natural periods. It can be concluded that the less the skirt diameter and skirt length, the higher the heave RAO. The results of this study show differences in motion characteristics of buoy geometries for both CB and SB, with their individual uniqueness.
3. The geometry has a significant effect on the added mass of an offshore structure, especially if it is symmetrical. At 0° flow angle, the CALM buoy formation is symmetrical in X and Y directions, for the square buoy (SB) and cylindrical buoy (CB). Thus, the total surface area is the same, which creates similar hydrodynamic behaviour in the sway and surge directions. As can be seen, the square buoy (SB) showed higher sway added mass and surge added mass than the cylindrical buoy (CB). For the pitch added mass, each buoy size had a unique similar relationship, as *SB* BuoySkirt1@13.90m had an identical pattern to *CB* BuoySkirt1@13.90m, and same for other buoy sizes. It can be observed that an increase in the buoy skirt size also increases the added mass, and this is expected. However, an increase in wave frequency will decrease this behaviour gradually. It can also be seen that the added mass components for the rotational components of the sway and surge motions.
4. From the pressure and motions analysis, it was observed that different flow angles have different effects on the CALM buoy. Using a structure interpolated pressure contours with pressure measured at the head of water, the contours in Sections 4.2.1-4.2.2 were generated. It shows the effect of flow angle on the hydrodynamics of the buoy. As the incident angle is from an angle, the hasher the effect of the waves on the CALM buoy. The study of the pressure and motion is important as it can be used to predict the motion behaviour and load transfer mode in the design of the CALM buoy.
5. The current speed is an important factor observed in this hydrodynamics study based on the waves-current interaction. It was observed

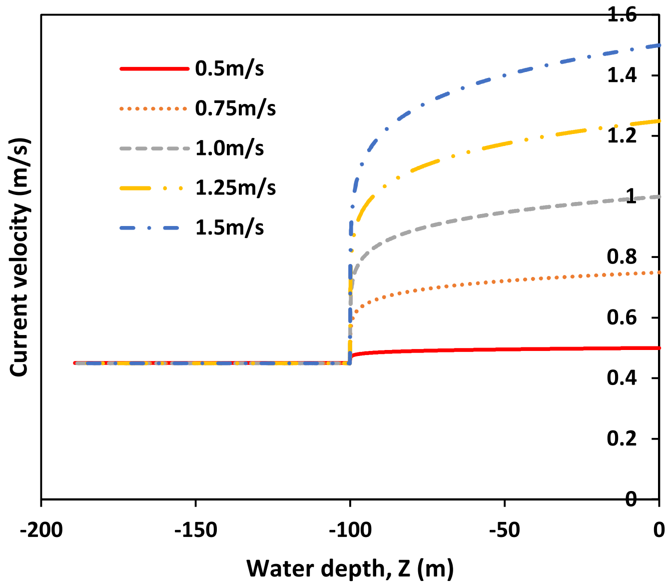

Fig. 39. The profiles for the current showing the five (5) current range considered in the parametric study in waves-current interaction study for the CALM buoy model in Section 4.2, across 0.5 m/s, 0.75 m/s, 1.0 m/s, 1.25 m/s and 1.5 m/s.

that as the current increases, the CALM buoy motion is influenced as it perturbates the submarine hoses. Also, the spectral density plots for the 6DoFs used in the investigation showed the characteristic behaviour of each motion form from the CALM buoy motion, influenced by the waves and current from the wave-current interaction.

6. From this study, increasing the surface current velocity decreases the bend radius (curvature) and also decreases the bend moment, which also increases the effective tension increases. An increase in seabed current velocity gives a reduced bend radius (Curvature), increased effective tension and bend moment. It can be observed that the surface wave is highly significant in the dynamic responses of the hose-line, the buoy stability and the buoy motion. Naturally, an increase in wave height, increases the dynamic responses of the submarine hoses. Thus, the significant height and zero-crossing period, are very sensitive in the buoy motion and can be investigated further. Further studies suggested is to include the investigation on the approximations analytically for the moving boundary of submarine hoses and the description of the moving boundary of submarine hoses, as such formulation is necessary for more understanding the stability and hydrodynamic behaviour of the CALM buoy.

5. Conclusion

With the increasing need for more sustainable offshore structures that are flexible, the use of CALM buoys has become more noticeable. This has been necessitated by the advances in computing techniques, effect of climate change, deep water exploration and adverse weather conditions. Thus, a relative increase in the modelling techniques used, such as the coupling model which has been presented on CALM buoys in the present model, as proposed. Numerical investigation on the motion characteristics of a CALM buoy has been successfully conducted in this study. The CALM buoy model was also validated. Next, the CALM buoy hydrodynamics, motion response, the effect of buoy skits and the effect of buoy geometries were investigated. Two types of buoys - square buoy (SB) and cylindrical buoy (CB), were considered to study the motion performance of both buoy forms. Detailed numerical investigation on CALM buoys with submarine hoses in Lazy-S configuration in 100m water depth, was then carried out. In this study, two different hydrodynamic panels were developed in ANSYS AQWA R2 2020 and solved using diffraction theory. The environmental conditions were based on a JONSWAP Wave Spectrum for five (5) environmental conditions, under irregular waves. The boundary conditions considered for the submarine hoses were attached on the PLEM and hose manifold underneath the CALM buoy. The RAOs obtained were then coupled into the Orcaflex FEM model developed based on Orcaflex Line theory. In addition, the model briefly presents the motion scenario when hoses are attached to the CALM buoy. The bending and deflection were analysed, as both parameters have an advantage in the prediction of the marine hose behaviour.

The model highlights include: hydrodynamic study on CALM buoy with results of RAO, radiation damping and added masses. Secondly is the coupled model carried out in two stages for offloading hose transfer. The RAO from ANSYS AQWA was loaded into Orcaflex in the dynamic process. This proposed method saves computing time, is cost-effective and has high accuracy. Thirdly, there is novelty in the two comparative studies based on buoy geometry (Square Buoy (SB) and the Cylindrical Buoy (CB)) and effect of buoy skirts for three dimensions of 13.90m, 12.90m and 11.90m. Fourthly, motion studies on the CALM buoy with spectral density plots for 6DoF were presented on the effects of waves and current angle on the global motion response of the CALM buoy hose system.

In conclusion, the numerical investigation involving static and dynamic analysis of a CALM buoy was conducted. From this investigation, some observations and recommendations made are detailed in Section 4.3. Notable findings from this investigation include the influence of buoy skirt dimensions and the buoy geometries on its hydrodynamic characteristics. Based on application with attachment, a particular aspect of motion response and position of CALM buoy based on the hydrodynamic loads was carried out on the effective tension and bending moment of the submarine hoses. It showed that current influences hose behaviour and detailed the wave-current interaction (WCI) studies on the CALM buoy system. The global response analysis on the effect of waves and current angle on the CALM buoy hose system was considered for wave-current interaction. The findings of this study included the incident angle, pressure from waves, and the buoy's deformation. These findings are aimed towards aiding the construction of buoys by buoy manufacturers and presents an understanding of floating buoys.

Data availability statement

The raw/processed data required to reproduce these findings cannot be shared at this time as the data also forms part of an ongoing study.

Funding

This research was funded by Engineering Department of Lancaster University, UK; Engineering and Physical Sciences Research Council (EPSRC)'s Doctoral Training Centre (DTC), UK; Standards Organisation of Nigeria (SON), Nigeria and Niger Delta Development Commission (NDDC), Nigeria. The financial support is highly appreciated. Also, the research reported in this paper is also part of the Projects 51922064 and 51879143 supported by the National Natural Science Foundation of China (NSFC). The authors hereby express immense gratitude to all the funders for supporting this research.

CRediT authorship contribution statement

Chiemela Victor Amaechi: Conceptualization, Methodology, Software, Validation, Formal analysis, Investigation, Resources, Data curation, Writing – original draft, preparation, Writing – review & editing, Visualization, Supervision, Project administration, Funding acquisition. **Facheng Wang:** Methodology, Validation, Investigation, Writing – review & editing, Supervision, Funding acquisition. **Jianqiao Ye:** Conceptualization, Methodology, Software, Validation, Investigation, Writing – review & editing, Supervision, Funding acquisition.

Declaration of competing interest

The authors declare that they have no known competing financial interests or personal relationships that could have appeared to influence the work reported in this paper.

Acknowledgement

The authors acknowledge the support of the Engineering Department of Lancaster University, UK; Standards Organisation of Nigeria (SON), Abuja and Niger Delta Development Commission (NDDC) Nigeria. The support from the user support team of the commercial software packages used- ANSYS and Orcina's Orcaflex, are also appreciated. The authors are very appreciative of the reviewers for their technical comments which have helped in improving the quality of this manuscript.

References

ABS, 2011. ABS Guidance: ABS Guidance Note on the Application of Fiber Rope for Offshore Mooring. American Bureau of Shipping (ABS), Houston, TX, USA.
ABS, 2014. ABS FPI: Rules for Building and Classing Floating Production Installations. American Bureau of Shipping (ABS), Houston, TX, USA.
ABS, 2021. Rules for Building and Classing - Single Point Moorings. American Bureau of Shipping, New York, USA. Available at: https://ww2.eagle.org/content/dam/eagle/rules-and-guides/current/offshore/8_rules-forbuildingandclassingsinglepointmoorings_2021/spm-rules-jan21.pdf, 21st September, 2021.
Amaechi, C.V., 2022. Novel Design, Hydrodynamics and Mechanics of Marine Hoses in Oil/gas Applications. PhD Thesis (in view). Lancaster University, Engineering Department, Lancaster, UK, 2021.
Amaechi, C.V., Ye, J., 2017. A numerical modeling approach to composite risers for deep waters. In: Ferreira, A.J.M., Larbi, W., Deu, J.-F., Tornabene, F., Fantuzzi, N. (Eds.), *ICCS20 20th International Conference On Composite Structures*; Structural and Computational Mechanics Book Series. Societa Editrice Esculapio, Bologna, Italy, pp. 262–263, 2017.
Amaechi, C.V., Ye, J., 2021k. Development of composite risers for offshore applications with review on design and mechanics. Ships Offshore Struct. 2021 (submitted for publication).
Amaechi, C.V., Ye, J., 2021l. A Review of State-Of-The-Art and Meta-Science Analysis on Composite Risers for Deep Seas. Ocean Engineering, 2021, under review.
Amaechi, C.V., Ye, J., 2021m. Local tailored design of deep water composite risers subjected to burst, collapse and tension loads. Ocean. Eng. 2021 https://doi.org/10.1016/j.oceaneng.2021.110196.
Amaechi, C.V., Wang, F., Hou, X., Ye, J., 2019a. Strength of submarine hoses in Chinese-lantern configuration from hydrodynamic loads on CALM buoy. Ocean Eng. 171, 429–442. https://doi.org/10.1016/j.oceaneng.2018.11.010, 2019.
Amaechi, C.V., Ye, J., Hou, X., Wang, F.-C., 2019b. Sensitivity studies on offshore submarine hoses on CALM buoy with comparisons for Chinese-lantern and Lazy-S configuration. Paper No.: OMAE2019-96755. In: 38th International Conference on Ocean, Offshore and Arctic Engineering, Glasgow, Scotland, June 9–14, 2019.
Amaechi, C.V., Odijie, A.C., Sotayo, A., Wang, F., Hou, X., Ye, J., 2019c. Recycling of renewable composite materials in the offshore industry. Encycl. Renew. Sustain. Mater. 2, 583–613. https://doi.org/10.1016/B978-0-12-803581-8.11445-6, 2019.
Amaechi, C.V., Odijie, A.C., Etim, O., Ye, J., 2019d. Economic aspects of fiber reinforced polymer composite recycling. Encycl. Renew. Sustain. Mater. 2, 377–397. https://doi.org/10.1016/B978-0-12-803581-8.10738-6, 2019.
Amaechi, C.V., Gillett, N., Odijie, A.C., Hou, X., Ye, J., 2019e. Composite risers for deep waters using a numerical modelling approach. Compos. Struct. 210, 486–499. https://doi.org/10.1016/j.compstruct.2018.11.057, 2019.
Amaechi, C.V., Gillett, N., Odijie, A.C., Wang, F., Hou, X., Ye, J., 2019f. Local and global design of composite risers on truss SPAR platform in deep waters. In: Proceedings of 5th International Conference on Mechanics of Composites, 2019, Paper No. 20005. Instituto Tecnico, Lisbon, Portugal, pp. 1–3 held from 1st -4th June, 2019, at.
Amaechi, C.V., Odijie, C.A., Wang, F., Ye, J., 2021a. Numerical investigation on mooring line configurations of a Paired Column Semisubmersible for its global performance in deep water condition. Ocean. Eng. 2021 (submitted for publication).
Amaechi, C.V., Wang, F., Ye, J., 2021m. Experiment and finite element modelling on the load response of offshore bonded loading hoses during reeling operation, normal operation and non-operation conditions. Ocean Eng. 2021, under review.
Amaechi, C.V., Wang, F., Ye, J., 2021b. Parametric investigation on tensioner stroke analysis, recoil analysis and disconnect for the marine drilling riser of a Paired Column Semisubmersible under deep water waves. Ocean. Eng. 2021, under review.
Amaechi, C.V., Wang, F., Ye, J., 2021c. Dynamic Analysis of Tensioner Model Applied on Global Response of Marine Riser Recoil and Disconnect. Marine Structures, 2021, under review.
Amaechi, C.V., Wang, F., Ye, J., 2021d. Effect of marine riser integration for characteristic motion response studies on a Paired Column Semisubmersible in deep waters. Mar. Struct. 2021 (submitted for publication).
Amaechi, C.V., Chesterton, C., Butler, H.O., Wang, F., Ye, J., 2021e. Review on the design and mechanics of bonded marine hoses for Catenary Anchor Leg Mooring (CALM) buoys, 2021 Ocean. Eng. 242 (7). https://doi.org/10.1016/j.oceaneng.2021.110062, 110062, 1-32.
Amaechi, C.V., Chesterton, C., Butler, H.O., Wang, F., Ye, J., 2021f. An overview on bonded marine hoses for sustainable fluid transfer and (Un)Loading operations via floating offshore structures (FOS). J. Mar. Sci. Eng. 9 (11), 1236. https://doi.org/10.3390/jmse9111236, 2021.
Amaechi, C.V., Wang, F., Ja'e, I.A., Aboshio, A., Odijie, A.C., Ye, J., 2021g. A literature review on the technologies of bonded hoses for marine applications. Ships and Offshore Structures, 2021, under review.
Amaechi, C.V., Wang, F., Ye, J., 2021h. Analytical cum numerical solutions on added mass and damping of a CALM buoy towards understanding the fluid-structure interaction of marine bonded hose under random waves. Mar. Struct. 2021 (submitted for publication).
Amaechi, C.V., Wang, F., Ye, J., 2021i. Understanding the fluid-structure interaction from wave diffraction forces on CALM buoys: numerical and analytical solutions. Ships Offshore Struct. 2021. https://doi.org/10.1080/17445302.2021.2005361.
Amaechi, C.V., Adelusi, I., Adefuye, E., Oyetunji, A.K., Ja'e, I.A., Wang, F., Ye, J., 2021j. Numerical study on plastic strain distributions and mechanical behaviour of a tube under bending. Inventions, 2021, under review.
Amaechi, C.V., Wang, F., Ye, J., 2021n. Experimental study on motion characterization of CALM buoy hose system with CFD investigation on vortex effect. J. Mar. Sci. Eng. 2021, under review.
Amaechi, C.V., Chesterton, C., Butler, H.O., Gu, Z., Odijie, C.A., Wang, F., Hou, X., Ye, J., 2021p. Finite element modelling on the mechanical behaviour of Marine Bonded Composite Hose (MBCH) under burst and collapse. J. Mar. Sci. Eng. 2021, under review.
Amaechi, C.V., Wang, F., Ye, J., 2021q. Investigation on hydrodynamic characteristics, wave-current interaction, and sensitivity analysis of submarine hoses attached to a CALM buoy. J. Mar. Sci. Eng. 2021 (submitted for publication).
Amaechi, C.V., Chesterton, C., Odijie, C.A., Ye, J., 2021r. Numerical assessment of marine hose load response during reeling and free-hanging operations under ocean waves. Mar. Struct. 2021, under review.
Amaechi, C.V., Wang, F., Ye, J., 2021s. Numerical assessment on the dynamic behaviour of submarine hoses attached to CALM buoy configured as Lazy-S under water waves, 2021 J. Mar. Sci. Eng. 9 (10), 1–48. https://doi.org/10.3390/jmse9101130, 1130.
Amaechi, C.V., Wang, F., Ye, J., 2021t. Mathematical modelling of bonded marine hoses for single point mooring (SPM) systems, with catenary anchor leg mooring (CALM) buoy application- A review, 2021 J. Mar. Sci. Eng. 9 (11), 1–62. https://doi.org/10.3390/jmse9111179, 1179.
ANSYS, 2017a. ANSYS Aqwa Theory Manual, Release 18.2. ANSYS Inc, Canonsburg, USA.
ANSYS, 2017b. ANSYS Aqwa User's Manual, Release 18.2. ANSYS Inc, Canonsburg, USA.
API, 2005. API RP 2SK: Recommended Practice for Design and Analysis of Station keeping Systems for Floating Structures, second ed. American Petroleum Institute (API), Washington, DC, USA.
API, 2007. API 2INT-MET: Interim Guidance on Hurricane Conditions in the Gulf of Mexico. American Petroleum Institute (API), Washington D.C., USA. Available at: https://law.resource.org/pub/us/cfr/ibr/002/api.2int-met.2007.pdf, 21st September, 2021.
API, 2013. API 17L2. Recommended Practice for Flexible Pipe Ancillary Equipment, first ed. American Petroleum Institute (API), Washington, DC, USA.
API, 2014. API RP 2SM: Design, Manufacture, Installation, and Maintenance of Synthetic Fiber Ropes for Offshore Mooring, second ed. American Petroleum Institute (API), Washington, DC, USA.
API, 2017. API 17K. Specification for Bonded Flexible Pipe. American Petroleum Institute (API), Washington, DC, USA.
API, 2021. API 17L2. Recommended Practice for Ancillary Equipment for Flexible Pipes and Subsea Umbilicals, second ed. American Petroleum Institute (API), Washington, DC, USA.
Aranha, J.A.P., Martins, M.R., 1997. Slender body approximation for yaw velocity terms in the wave drift damping matrix. In: International Workshop on Water Waves and Floating Bodies - IWWWFB97. Marseilles, France: IWWWFB, pp. 1–7. Available at: http://www.iwwwfb.org/Abstracts/iwwwfb12/iwwwfb12_01.pdf (Accessed on: 21st September, 2021).
Bai, Y., Bai, Q., 2005. Subsea Pipelines and Risers, first ed. Elsevier, Oxford, UK.
Berhault, C., Guérin, P., Le Buhan, P., Heurtier, J.M., 2004. Investigations on hydrodynamic and mechanical coupling effects for deepwater offloading buoy. In: Paper Presented at the the Fourteenth International Offshore and Polar Engineering Conference, May 23–28, 2004. Toulon, France.
Berteaux, H.O., 1976. Buoy Engineering, first ed. John Wiley and Sons, New York, USA.
Bhatta, D.D., Rahman, M., 2003. On scattering and radiation problem for a cylinder in water of finite depth. Int. J. Eng. Sci. 41, 931–967. https://doi.org/10.1016/S0020-7225(02)00381-6.
Bidgoli, S.I., Shahriari, S., Edalat, P., 2017. Sensitive analysis of different types of deep water risers to conventional mooring systems. Int. J. Coast. Offshore Eng. 5, 45–55. Available at: https://ijcoe.org/article-1-90-en.pdf, 5th November, 2021.
Bishop, R.E.D., Johnson, D.C., 2011. *The Mechanics Of Vibration.* 1960 Reprint, first ed. Cambridge University Press, Cambridge, UK.
Bishop, R.E.D., Price, W.G., 2005. *Hydroelasticity Of Ships.* 1979 Reprint, first ed. Cambridge University Press, New York, USA.
Bluewater, 2011. *Bluewater turret buoy- technical description*, amsterdam, The Netherlands: bluewater energy services. Available at: https://www.bluewater.com/wp-content/uploads/2013/04/digitale-brochure-TurretBouy-Tech-description.pdf, 12th November, 2020.

Boo, S.Y., Shelley, S.A., 2021. Design and analysis of a mooring buoy for a floating arrayed WEC platform. Processes 9 (8), 1390. https://doi.org/10.3390/pr9081390, 2021.

Brady, I., Williams, S., Golby, P., 1974. A study of the forces acting on hoses at a monobuoy due to environmental conditions. In: Offshore Technology Conference Proceeding -OTC 2136. Dallas, Texas, USA: OnePetro, May 5–7, 1974, pp. 1–10. https://doi.org/10.4043/2136-MS 10.4043/2136-MS.

Brebbia, C.A., Dominguez, J., 1977. Boundary element methods for potential problems. Appl. Math. Model. 1 (7), 372–378. https://doi.org/10.1016/0307-904X(77)90046-4, 1977.

Brebbia, C.A., Walker, S., 2013. Dynamic Analysis of Offshore Structures, first ed. Newnes-Butterworth & Co. Publishers Ltd, London, UK, p. 1979. Reprint.

Bree, J., Halliwell, A.R., Tom, O'Donoghue, 1989. Snaking of floating marine oil hose attached to SPM buoy. J. Eng. Mech. 115 (2), 265–284. https://doi.org/10.1061/(ASCE)0733-9399(1989)115:2(265).

Bridgestone, J., 1976. Study of Causes of Kinking in Floating Hoses at Petrobras/Tefran Terminal. Report No. 6YMT-0011, Japan.

Brown, M.J., 1985a. Mathematical model of a marine hose-string at a buoy- Part 1 - static problem. In: Dyke, P., Moscardini, A.O., Robson, E.H. (Eds.), Offshore and Coastal Modelling. Springer, England, pp. 251–277. https://doi.org/10.1007/978-1-4684-8001-6_14.

Brown, M.J., 1985b. Mathematical model of a marine hose-string at a buoy- Part 2 - dynamic problem. In: Dyke, P., Moscardini, A.O., Robson, E.H. (Eds.), Offshore and Coastal Modelling. Springer, England, pp. 279–301. https://doi.org/10.1007/978-1-4684-8001-6_13.

Brown, M.J., Elliott, L., 1987. A design tool for static underbuoy hose-systems. Appl. Ocean Res. 9 (3), 171–180. https://doi.org/10.1016/0141-1187(87)90021-6.

Brown, M.J., Elliott, L., 1988. Two-dimensional dynamic analysis of a floating hose string. Appl. Ocean Res. 10 (1), 20–34. https://doi.org/10.1016/S0141-1187(88)80021-X.

Brown, A., Gorter, W., Paalvast, M., Kymmell, J., 2016. Design approach for CALM buoy moored vessel in Squall conditions. In: Proceedings of the ASME 2016 35th International Conference on Ocean, Offshore and Arctic Engineering. Volume 1: *Offshore Technology; Offshore Geotechnics*. Busan, South Korea. June 19–24, 2016. V001T01A012. ASME. https://doi.org/10.1115/OMAE2016-54826.

Brown, A., Gorter, W., Vanderschuren, L., Tromans, P., Jonathan, P., Verlaan, P., 2017. Design approach for turret moored vessels in highly variable Squall conditions. In: Proceedings of the ASME 2017 36th International Conference on Ocean, Offshore and Arctic Engineering. Volume 3A*: Structures, Safety And Reliability*. Trondheim, Norway. June 25–30, 2017. V03AT02A049. ASME. https://doi.org/10.1115/OMAE2017-61005.

Bunnik, T.H.J., de Boer, G., Cozijn, J.L., van der Cammen, J., van Haaften, E., ter Brake, E., 2002. Coupled mooring analysis and large scale model tests on a deepwater calm buoy in mild wave conditions. In: Proceedings of the ASME 2002 21st International Conference on Offshore Mechanics and Arctic Engineering. 21st International Conference on Offshore Mechanics and Arctic Engineering, Volume 1. Oslo, Norway. June 23–28. ASME, pp. 65–76. https://doi.org/10.1115/OMAE2002-28056, 2002.

Chakrabarti, S.K., 1972. Nonlinear wave forces on vertical cylinder. J. Hydraul. Division, Proc. Am. Soc. Civil Eng. 102 (HY11). November 1972.

Chakrabarti, S.K., 1975. Second-order wave force on large vertical cylinder. J. Waterw. Harb. Coast. Eng. Div. 101 (3), 311–317.

Chandrasekaran, S., 2015. Dynamic Analysis and Design of Offshore Structures, first ed. Springer, New Delhi, India.

Chandrasekaran, S., Jain, A.K., 2002. Dynamic behaviour of square and triangular offshore tension leg platforms under regular wave load. Ocean. Eng. 29 (3), 279–313. https://doi.org/10.1016/S0029-8018(00)00076-7.

Chandrasekaran, S., Jain, A.K., Chandak, N.R., 2007. Response behavior of triangular tension leg platforms under regular waves using Stokes nonlinear wave theory. J. Waterw. Port, Coast. Ocean Eng. 133 (3), 230–237. https://doi.org/10.1061/(ASCE)0733-950X(2007)133:3(230).

Chen, L., Basu, B., 2018. Wave-current interaction effects on structural responses of floating offshore wind turbines. Wind Energy 22, 327–339. https://doi.org/10.1002/we.2288, 2019.

Cozijn, Cozijn, J.L., Bunnik, T.H.J., Parts, A., Vancouver, B., 2004. Coupled mooring analysis for a deep water CALM buoy. In: Proceedings Of the ASME 2004 23rd International Conference On Offshore Mechanics And Arctic Engineering. 23rd International Conference On Offshore Mechanics And Arctic Engineering, vol. 1. ASME, pp. 663–673. https://doi.org/10.1115/OMAE2004-51370. British Columbia, Canada. June 20–25, 2004.

Cozijn, H., Uittenbogaard, R., Brake, E. Ter, 2005. Heave , roll and pitch damping of a deepwater CALM buoy with a skirt. In: *International Society Of Offshore And Polar Engineering Conference* (ISOPE) *Proceedings. Seoul, Korea, 19–24 June 2005*, vol. 8. ISOPE, Cupertino, CA, USA, pp. 388–395. Available at: https://www.researchgate.net/publication/267364857_Heave_Roll_and_Pitch_Damping_of_a_Deepwater_CALM_Buoy_with_a_Skirt. (Accessed 11 September 2021).

Dareing, D.W., 2012. Mechanics of Drillstrings and Marine Risers. ASME Press, New York, USA. https://doi.org/10.1115/1.859995.

Demirbilek, Z., Gaston, J.D., 1985. Nonlinear wave loads on a vertical cylinder. Ocean Eng. 12 (5), 375–385. https://doi.org/10.1016/0029-8018(85)90001-0, 1985.

Denney, D., 2006. Chain failure by bending on deepwater mooring systems, 02 J. Petrol. Technol. 58, 72–73. https://doi.org/10.2118/0206-0072-JPT. Paper Number: SPE-0206-0072-JPT.

DNV, 2013. Offshore Standard—Position Mooring; DNV OS-E301; Det Norske Veritas (DNV): Høvik. Norway, 2013.

DNVGL, 2015. *DNVGL-OS-E403 Offshore loading buoys*, oslo, Norway: det norske Veritas & germanischer Lloyd. Available at: https://rules.dnv.com/docs/pdf/DNV/os/2015-07/DNVGL-OS-E403.pdf, 6th July, 2021.

DNVGL, 2016. *DNVGL-OS-E403 Offshore loading units*, oslo, Norway: det norske Veritas & germanischer Lloyd. Available at: https://rules.dnv.com/docs/pdf/DNV/OS/2016-04/DNVGL-OS-E403.pdf, 6th July, 2021.

DNVGL, 2017. DNVGL-RP-F205 *Global Performance Analysis of Deepwater Floating Structures*, Oslo, Norway. Det Norske Veritas & Germanischer Lloyd.

Duggal, A., Ryu, S., 2005. The dynamics of deepwater offloading buoys. In: WIT Transactions on the Built Environment. Paper FSI05026FU. WIT Press, Singapore. https://www.witpress.com/Secure/elibrary/papers/FSI05/FSI05026FU.pdf, 6th July, 2021.

Duggal, A., Heyl, C., Izadparast, A.H., Minnebo, J., 2011. Response of FPSO systems to squalls. In: Proceedings Of the ASME 2011 30th International Conference On Ocean, Offshore And Arctic Engineering, vol. 3. ASME, pp. 913–920. https://doi.org/10.1115/OMAE2011-49855. Materials Technology; Jan Vugts Symposium on Design Methodology of Offshore Structures; Jo Pinkster Symposium on Second Order Wave Drift Forces on Floating Structures; Johan Wichers Symposium on Mooring of Floating Structures in Waves. Rotterdam, The Netherlands. June 19–24, 2011.

Edalat, P., Hasanvand, E., 2021a. Technical comparison of offshore oil terminals under the effect of the Persian Gulf environmental conditions. J. Mar. Sci. Technol. https://doi.org/10.22113/jmst.2021.233123.2374, 2021, URL: http://jmst.sinaweb.net/article_133843.html?lang=en, 5th November, 2021.

Edalat, P., Hasanvand, E., 2021b. Mooring system fatigue analysis for CALM and SALM oil terminals. Int. J. Maritime Technol. (ijmt) 15, 51–65. URL: http://ijmt.ir/article-1-741-en.html, 5th November, 2021.

Edward, C., Kr Dev, D.A., 2021. Assessment of CALM buoys motion response and dominant OPB/IPB inducing parameters on fatigue failure of offshore mooring chains. In: Okada, T., Suzuki, K., Kawamura, Y. (Eds.), Practical Design of Ships and Other Floating Structures. PRADS 2019, Lecture Notes in Civil Engineering, vol. 64. Springer, Singapore. https://doi.org/10.1007/978-981-15-4672-3_35.

Esmailzadeh, E., Goodarzi, A., 2001a. Stability analysis of a CALM floating offshore structure. Int. J. Non-Linear Mech. 36 (6), 917–926. https://doi.org/10.1016/S0020-7462(00)00055-X.

Faltinsen, O.M., 1990. *Sea Loads On Ships And Offshore Structures* 1995 Repri. Cambridge University Press, Cambridge, UK.

Garrison, C.J., 1974. Hydrodynamics of large objects in the sen; Part I: hydrodynamic analysis. J. Hydronautics 8, 5–12. https://doi.org/10.2514/3.62970, 1974.

Garrison, C.J., 1975. Hydrodynamics of large objects in the sea; Part II: motion of free floating bodies. J. Hydronautics 9 (2), 58–63. https://doi.org/10.2514/3.63020, 1975.

Garrison, C.J., 1979. The Consistent Second-Order Theory of Wave/Structure Interaction. Report Number FEDDOCS D 208.14/2: NPS-69-79-010. Naval Postgraduate School, Research Reports Division, Monterey, California, USA, pp. 1–42. Available at: https://core.ac.uk/download/pdf/36722593.pdf. Assessed on: 16th May, 2021.

Garrison, C.J., 1984. Nonlinear wave loads on Large structures. In: Proc. Third Int. Offshore Mechanics and Arctic Engineering (OMAE) Symposium, ASME, 1, pp. 128–135, 1984.

Ghalayini, Williams, 1991. Nonlinear wave forces on vertical cylinder arrays. J. Fluid Struct. 5 (1), 1–32. https://doi.org/10.1016/0889-9746(91)80009-3. January 1991.

Gu, H., 2016. Coupled Mooring Analysis of a CALM Buoy by a CFD Approach. Masters Thesis, Texas A&M University, USA. Available at: https://core.ac.uk/download/pdf/79654768.pdf, 6th July, 2021.

Gu, H., Chen, H.-C., Zhao, L., 2017. Coupled mooring analysis of a CALM buoy by a CFD approach. In: Paper Presented at the the 27th International Ocean and Polar Engineering Conference, San Francisco, California, USA, June 2017. Paper Number: ISOPE-I-17-223. Available at: https://onepetro.org/ISOPEIOPEC/proceedings-abstract/ISOPE17/All-ISOPE17/ISOPE-I-17-223/17484, 6th July, 2021.

Gu, Haoyuan, Chen, Hamn-Ching, Zhao, Linyue, 2019. Coupled CFD-FEM simulation of hydrodynamic responses of a CALM buoy. Ocean Syst. Eng. 9 (1), 21–42. https://doi.org/10.12989/ose.2019.9.1.021. March 2019.

Hasanvand, E., Edalat, P., 2020. Sensitivity analysis of the dynamic response of CALM oil terminal, in the Persian Gulf region under different operation parameters. J. Mar. Eng. 16 (32), 73–84. https://doi.org/10.29252/marineeng.16.32.73, 2020. http://marine-eng.ir/article-1-794-en.html, 5th November, 2021.

Hasanvand, E., Edalat, P., 2021a. Evaluation of the safe and failure zones of mooring and riser systems in a CALM oil terminal. J. Mar. Sci. Appl. https://doi.org/10.1007/s11804-021-00240-z, 2021.

Hasanvand, E., Edalat, P., 2021b. A comparison of the dynamic response of a product transfer system in CALM and SALM oil terminals in operational and non-operational modes in the Persian Gulf region, 2021 Int. J. Coast. Offshore Eng. 5 (1), 1–14. Available at: http://ijcoe.org/article-1-232-en.pdf, 5th November, 2021.

Hasanvand, E., Edalat, P., 2021c. Comparison of dynamic response of Chinese lantern and Lazy-S riser configurations used in CALM oil terminal, 2021 Mar. Eng. 17, 37–52 [In: Persian Language]. URL: http://marine-eng.ir/article-1-857-en.html, 5th November, 2021.

Havelock, T.H., 1940. The pressure of water waves upon a fixed obstacle. In: Proceedings of the Royal Society of London. Series A , Mathematical and Physical Sciences, 175, pp. 409–421. https://doi.org/10.1098/rspa.1940.0066, 963.

Hirdaris, S.E., Bai, W., Dessi, D., Ergind, A., Gu, X., Hermundstad, O.A., Huijsmans, R., Iijima, K., Nielsen, U.D., Parunov, J., Fonseca, N., Papanikolaou, A., Argyriadis, K., Incecik, A., 2014. Loads for use in the design of ships and offshore structures. Ocean Eng. 78, 131–174. https://doi.org/10.1016/j.oceaneng.2013.09.012.

Huang, T.S., Leonard, J.W., 1989. *Lateral Stability of a flexible submarine hoseline*, Port Hueneme, California, USA. Available at: https://apps.dtic.mil/sti/pdfs/ADA219251.pdf, 8th September, 2021.

Huang, T.S., Leonard, J.W., 1990. Lateral Stability of a submarine flexible hoseline. Ocean Eng. 17 (1–2), 35–52. https://doi.org/10.1016/0029-8018(90)90013-V, 1990.

Irvine, H.M., 1981. Cable Structures. MIT Press, Cambridge, Massachusetts, USA.

ITTC, 1987. Discussions: OE1- Koterayama W.- Wave Forces Acting on a Vertical Circular Cylinder with a Constant Forward Velocity: Report of the Ocean Engineering Committee, 18th ITTC (1987). Available at: https://ittc.info/media/2590/session-on-ocean-engineering.pdf, 8th September, 2021.

ITTC, 2002. The specialist committee on waves - final report and recommendations to the 23rd ITTC. 23rd international towing tank conference. In: Proceedings of the 23rd ITTC-Volume, vol. 11, pp. 505–736. Available at: https://ittc.info/media/1469/waves.pdf, 8th September, 2021.

Jacobsen, L.S., 1949. Impulsive hydrodynamics of fluid inside a cylindrical tank and of fluid surrounding a cylindrical pier. Bull. Seismol. Soc. Am. 39 (3), 189–204. https://doi.org/10.1785/BSSA0390030189.

Jain, A.K., 1997. Nonlinear coupled response of offshore tension leg platform to regular wave forces. Ocean. Eng. 24 (No. 7), 577–593. https://doi.org/10.1016/0029-8018(95)00059-3.

Jean, P., Goessens, K., L'Hostis, D., 2005. Failure of chains by bending on deepwater mooring systems. In: Paper Presented at the Offshore Technology Conference, Houston, Texas, May 2005. Paper Number: OTC-17238-MS. https://doi.org/10.4043/17238-MS.

Kang, Y., Sun, L., Kang, Z., Chai, S., 2014. Coupled analysis of FPSO and CALM buoy offloading system in West Africa. In: Proceedings of the ASME 2014 33rd International Conference on Ocean, Offshore and Arctic Engineering. Volume 8A: Ocean Engineering. San Francisco, California, USA. June 8–13, 2014. V08AT06A010. ASME. https://doi.org/10.1115/OMAE2014-23118.

Kang, Z., Zhang, C., Ni, W., Xu, X., 2017. Research on hydrodynamic calculation method of deepwater CALM buoy. In: International Ocean and Polar Engineering. ISOPE, San Francisco, California, USA, pp. 217–224. Available at: http://legacy.isope.org/publications/proceedings/ISOPE/ISOPE%202017/data/64789-isope-vol3-1.3611459/t001-1.3612712/f004-1.3613031/a033-1.3613035.html, 8th September, 2021.

Kashiwagi, M., 2000. Hydrodynamic interactions among a great number of columns supporting a very large flexible structure. J. Fluid Struct. 14 (7), 1013–1034. https://doi.org/10.1006/jfls.2000.0306. October 2000.

Kim, Y., Sclavounos, P.D., 1998. A finite-depth unified theory of ship motion. In: International Workshop on Water Waves and Floating Bodies. IWWWFB, Delft, Netherlands, pp. 71–74. Available at: http://www.iwwwfb.org/%5C/Abstracts/iwwwfb13/iwwwfb13_19.pdf, 8th January, 2021.

Koterayama, W., 1984. Wave forces acting on a vertical circular cylinder with a constant forward velocity. Ocean Eng. 11 (4).

Le Cunff, C., Ryu, S., Duggal, A.S., Ricbourg, C., Heurtier, J., Heyl, C., Liu, Y., Beauclair, O., 2007. Derivation of CALM buoy coupled motion RAOs in frequency domain and experimental validation. In: International Society of Offshore and Polar Engineering Conference Proceedings. ISOPE, Lisbon, Portugal, pp. 1–8. Available at: https://www.sofec.com/wp-content/uploads/white_papers/2007-ISOPE-Derivation-of-CALM-Buoy-Coupled-Motion-RAOs-in-Frequency-Domain.pdf. (Accessed 11 September 2021).

Le Cunff, C., Ryu, S., Heurtier, J., Duggal, A.S., 2008. Frequency-domain calculations of moored vessel motion including low frequency effect. In: Proceedings of the ASME 2008 27th International Conference on Offshore Mechanics and Arctic Engineering. Volume 1: Offshore Technology. Estoril, Portugal. June 15–20, 2008. ASME, pp. 689–696. https://doi.org/10.1115/OMAE2008-57632.

Lebon, L., Remery, J., 2002. Bonga: oil off-loading system using flexible pipe. In: Offshore Technology Conference Proceeding -OTC 14307. OnePetro, Houston, Texas, USA, pp. 1–12. https://doi.org/10.4043/14307-MS.

Lenci, S., Callegari, M., 2005. Simple analytical models for the J-lay problem. Acta Mech. 39, 23–39. https://doi.org/10.1007/s00707-005-0239-x.

Lighthill, J., 1979. Waves and hydrodynamic loading. In: Proc. 2nd. Int. Conf. Behavior of Offshore Structures (BOSS '79). London, pp. 1–40.

Lighthill, J., 1986. Fundamentals concerning wave loading on offshore structures. J. Fluid Mech. 173 (1), 667–681. https://doi.org/10.1017/S0022112086001313.

Liu, B., Fu, D., Zhang, Y., Chen, X., 2020. Experimental and numerical study on the wave force calculation of a partially immersed horizontal cylindrical float. Int. J. Naval Archit. Ocean Eng. 12 (2020), 733–742. https://doi.org/10.1016/j.ijnaoe.2020.08.002.

Lucas, C., Guedes Soares, C., 2015. Bivariate distributions of significant wave height and mean wave period of combined sea states. Ocean. Eng. 106, 341–353. https://doi.org/10.1016/j.oceaneng.2015.07.010.

Luongo, A., Zulli, D., 2013. *Mathematical Models Of Beams And Cables*. Mechanical Engineering and Solid Mechanics Series, first ed. Wiley-ISTE Imprint, John Wiley & Sons, Inc., USA https://doi.org/10.1002/9781118577554.

MacCamy, R.C., Fuchs, R.A., 1954. *Wave Forces on Piles: a Diffraction Theory*, Report BEB-TM-69, Beach Erosion Board. Department of Army, USA. Washington D.C., USA, pp. 1–17. Available at: https://erdc-library.erdc.dren.mil/jspui/bitstream/11681/3444/1/BEB-TM-69.pdf, 8th September, 2021.

Mohamed, H.A.M.A., 2011. Hydrodynamic Loading and Responses of Semisubmersibles. Ph.D Thesis. School of Marine Science and Technology, Newcastle University, Newcastle upon Tyne, UK. Available at: https://theses.ncl.ac.uk/jspui/bitstream/10443/1285/1/Hassan%20Mohamed%2011.pdf, 6th October, 2021.

Morison, J.R., Johnson, J.W., Schaaf, S.A., 1950. The force exerted by surface waves on piles. *Petroleum transactions,* paper number: SPE-950149-G. *AIME*, 189. J. Petrol. Technol. 2, 149–154. https://doi.org/10.2118/950149-G, 05.

Newman, J.N., 1979. Absorption of wave energy by elongated bodies. Appl. Ocean Res. 1 (4), 189–196. https://doi.org/10.1016/0141-1187(79)90026-9. October 1979.

Newman, J.N., 1994. Wave effects on deformable bodies. Appl. Ocean Res. 16 (1), 47–59. https://doi.org/10.1016/0141-1187(94)90013-2, 1994.

Newman, J.N., 1996. The second-order wave force on a vertical cylinder. J. Fluid Mech. 320, 417–443. https://doi.org/10.1017/S0022112096007598.

Newman, J.N., Lee, C.-H., 2002. Boundary-element methods in offshore structure analysis. J. Offshore Mech. Arctic Eng. 124 (May 2002), 81–89. https://doi.org/10.1115/1.1464561.

O'Donoghue, T., 1987. The Dynamic Behaviour of a Surface Hose Attached to a CALM Buoy. Ph.D Thesis. Heriot-Watt University, Edinburgh, U.K, 1987. Available at: https://www.ros.hw.ac.uk/handle/10399/1045?show=full, 17th May 2021.

O'Donoghue, T., Halliwell, A.R., 1988. Floating hose-strings attached to A calm buoy. In: Offshore Technology Conference, Houston, Texas, May 1988. Paper Number: OTC-5717-MS. https://doi.org/10.4043/5717-MS.

OCIMF, 1995a. Single Point Mooring Maintenance and Operations Guide (SMOG). Witherby & Co. Ltd, London, UK.

OCIMF, 1995b. Guideline for the Handling, Storage, Inspection and Testing of the Hose, second ed. Witherby & Co. Ltd, London, UK.

OCIMF, 2009. Guide to Manufacturing and Purchasing Hoses for Offshore Moorings (GMPHOM). Witherby Seamanship International Ltd, Livingstone, UK.

OCIMF, 2020. A study into crane loads associated with hose handling at offshore terminals, OCIMF info paper, version 6. Oil Companies international marine Forum (OCIMF). London, UK. Available at: https://www.ocimf.org/media/58339/OC_INFOPAPER2961_CRANE_V6.pdf, 14th February, 2021.

Odijie, A.C., 2016. Design of Paired Column Semisubmersible Hull. Ph.D Thesis, Lancaster University, Engineering Department, Lancaster, UK. Available at: https://eprints.lancs.ac.uk/id/eprint/86961/1/2016AgbomeriePhD.pdf, 12th Feb., 2021.

Odijie, A.C., Ye, J., 2015a. Effect of vortex induced vibration on a paired-column SemiSubmersible platform. Int. J. Struct. Stabil. Dynam. 15 (8) https://doi.org/10.1142/s0219455415400192.

Odijie, A.C., Ye, J., 2015b. Understanding Fluid-Structure Interaction for high amplitude wave loadings on a deep-draft paired column semi-submersible platform: a finite element approach. In: International Conference on Light Weight Design of Marine Structures, Glasgow, UK. https://doi.org/10.13140/RG.2.1.3259.5283, 17th May, 2016.

Odijie, A.C., Quayle, S., Ye, J., 2017a. Wave induced stress profile on a paired column semisubmersible hull formation for column reinforcement. Eng. Struct. 143 (April), 77–90. https://doi.org/10.1016/j.engstruct.2017.04.013.

Odijie, A.C., Wang, F., Ye, J., 2017b. A review of floating semisubmersible hull systems: column stabilized unit. Ocean Eng. 144 (October 2016), 191–202. https://doi.org/10.1016/j.oceaneng.2017.08.020. Available at:

Orcina, 2014. OrcaFlex Manual, Version 9.8a, Ulverton. Orcina Ltd, Cumbria, UK.

Orcina, 2020. Orcaflex documentation, version 11.0f. Available at: https://www.orcina.com/webhelp/OrcaFlex/Default.htm, 16th February, 2020.

Orcina, 2021. Orcaflex -dynamic analysis software for offshore marine systems. Orcaflex help manual. Orcina, ulverston, UK. Available at: https://www.orcina.com/SoftwareProducts/OrcaFlex/Documentation/index.php, 11th July, 2021.

O'Donoghue, T., Halliwell, A.R., 1990. Vertical bending moments and axial forces in a floating marine hose-string. Eng. Struct. 12 (4), 124–133. https://doi.org/10.1016/0141-0296(90)90018-N.

Paalvast, M., Kymmell, J., Gorter, W., Brown, A., 2016. Response of a CALM buoy moored vessel in Squall condition. In: Proceedings of the ASME 2016 35th International Conference on Ocean, Offshore and Arctic Engineering. Volume 1: *Offshore Technology; Offshore Geotechnics*. Busan, South Korea. June 19–24, 2016. V001T01A059. ASME. https://doi.org/10.1115/OMAE2016-54968 Available at. https://www.mocean-offshore.com/wp-content/uploads/2016/04/OMAE2016-54968.pdf, 17th December, 2021).

Pham, T.D., Shin, H., 2019. A new conceptual design and dynamic analysis of a spar-type offshore wind turbine combined with a moonpool. Energies 12 (19), 3737. https://doi.org/10.3390/en12193737, 2019.

Pinkster, J.A., Remery, G.F.M., 1975. The role of model tests in the design of single point mooring terminals. In: Offshore Technology Conference Proceeding -OTC 2212. OnePetro, Dallas, Texas, USA, pp. 679–702. https://doi.org/10.4043/2212-MS.

Qi, X., Chen, Y., Yuan, Q., Xu, G., Kevin, H., 2017. CALM buoy and fluid transfer system study. In: International Offshore and Polar Engineering Conference. ISOPE, San Francisco, California, USA, pp. 932–939. Available at: https://onepetro.org/ISOPEIOPEC/proceedings-abstract/ISOPE17/All-ISOPE17/ISOPE-I-17-128/17225, 16th February, 2021.

Quash, J.E., Burgess, S., 1979. Improving underbuoy hose system design using relaxed storm design criteria. In: Offshore Technology Conference Proceeding. April 30–May 3, 1979, Houston, Texas, USA, pp. 1827–1836. https://doi.org/10.4043/3565-MS.

Rahman, M., 1981. Non-linear wave loads on large circular cylinders: a perturbation technique. Adv. Water Resour. 4 (1), 9–19. https://doi.org/10.1016/0309-1708(81)90003-8.

Rahman, M., 1984. Second order wave interaction with large structures. In: Rogers, T.B.M.C. (Ed.), Wave Phenomena: Modern Theory and Applications. Elsevier B.V., Holland, pp. 49–69. https://doi.org/10.1016/S0304-0208(08)71254-4. North-Holland Mathematics Studies. Volume 97, 1984, Pages 49-69.

Rahman, M., Chakravartty, I.C., 1981. Hydrodynamic loading calculations for offshore structures. SIAM J. Appl. Math. 41 (3), 445–458. https://doi.org/10.1137/0141037.

Raman, H., Venkatanarasaiah, 1976. Forces due to nonlinear waves on vertical cylinders. J. Waterways Harbors Coast. Eng. Div. Proc. Am. Soc. Civil Eng. 102 (WW3) https://doi.org/10.1061/AWHCAR.0000331. August 1976.

Raman, H., Jothi Shankar, N., Venkatanarasaiah, P., 1977. Nonlinear wave interaction with vertical cylinder of large diameter. J. Ship Res., SNAME 21 (No. 2), 120–124. https://doi.org/10.5957/jsr.1977.21.2.120.

Ricbourg, C., Berhault, C., Camhi, A., Lécuyer, B., Marcer, R., 2006. Numerical and experimental investigations on deepwater CALM buoys hydrodynamics loads. In: Offshore Technology Conference Proceeding -OTC 18254 -*PP*. May 1–4, 2006. Houston, Texas, USA: OnePetro, pp. 1–8. https://doi.org/10.4043/18254-MS.

Rodríguez, G., Guedes Soares, C., 1999. The bivariate distribution of wave height and periods in mixed sea states. ASME J. Offshore Mech. Arctic Eng. 121 (2), 102–108. https://doi.org/10.1115/1.2830073.

Roveri, F.E., Sudati Sagrilo, Luís Volnei, Cicilia, F.B., 2002. A case study on the evaluation of floating hose forces in a C.A.L.M. System. In: International Offshore and Polar Engineering Conference. Kitakyushu, Japan,: ISOPE, pp. 190–197. Available online: https://onepetro.org/ISOPEIOPEC/proceedings-abstract/ISOPE02/All-ISOPE02/ISOPE-I-02-030/8329, 17th July, 2021.

RPSEA, 2009. Ultra deepwater dry tree system for drilling and production. Research Partnership to Secure Energy for America (RPSEA), USA. NETL's Energy Data eXchange. Available at: https://edx.netl.doe.gov/dataset/ultra-deepwater-dry-tree-system-for-drilling-and-production/resource/ada36673-a4c9-4e92-9e78-05003fe9c9d4/download/07121-1402a-FR-Ultra-Deepwater_Dry_Tree_System_Drilling_Production_GOM-06-19-09_P.pdf, 6th September, 2021.

Rueda-Bayona, J.G., Guzmán, A., Cabello Eras, J.J., 2020. Selection of JONSWAP spectra parameters during water-depth and sea-state transitions. J. Waterw. Port, Coast. Ocean Eng. 146 (6), 04020038 https://doi.org/10.1061/(ASCE)WW.1943-5460.0000601.

Ryu, S., Duggal, A.S., Heyl, C.N., Liu, Y., 2006. Prediction of deepwater oil offloading buoy response and experimental validation. Int. J. Offshore Polar Eng. 16 (3), 1–7. Available at: https://www.sofec.com/wp-content/uploads/white_papers/2006-ISOPE-Prediction-of-DW-Oil-Offloading-Buoy-Response.pdf. (Accessed 11 September 2021).

Saito, H., Mochizuki, T., Fukai, T., Okui, K., 1980. Actual measurement of external forces on marine hoses for SPM. In: Offshore Technology Conference Proceeding -OTC 3803. May 5–8, 1980. Houston, Texas, USA: OnePetro, pp. 89–97. https://doi.org/10.4043/3803-MS.

Salem, A.G., Ryu, S., Duggal, A.S., Datla, R.V., 2012. Linearization of quadratic drag to estimate CALM buoy pitch motion in frequency-domain and experimental validation. In: Presented in 28th International Conference on Ocean, Offshore and Arctic Engineering (OMAE), May 31-June 5, 2009, Honolulu, Hawaii. Published in: ASME. *J. Offshore Mech. Arct. Eng.* February, vol. 134, 011305. https://doi.org/10.1115/1.4003645, 2012, 1. Available at: https://www.sofec.com/wp-content/uploads/white_papers/2009-OMAE-80212-Linearization-Quad-Drag-Est-CALM-Pitch-Motion-in-F-D-Exp-Validation-.pdf (Accessed on: 11 September 2021).

Sarpkaya, T., 2014. Wave Forces on Offshore Structures, first ed. Cambridge University Press, New York, USA.

Sorensen, R.M., 1993. Basic Wave Mechanics: for Coastal and Ocean Engineers. John Wiley and Sons.

Sorensen, R.M., 2006. Basic Coastal Engineering, third ed. Springer, New York, USA.

Sparks, C.P., 2018. Fundamentals of Marine Riser - Basic Principles and Simplified Analyses, second ed. PennWell Books, Oklahoma, USA.

Sun, L., Zhang, X., Kang, Y., Chai, S., 2015. Motion response analysis of FPSO's CALM buoy offloading system. In: Proceedings of the ASME 2015 34th International Conference on Ocean, Offshore and Arctic Engineering. Volume 11: *Prof. Robert F. Beck Honoring Symposium On Marine Hydrodynamics*. St. John's, Newfoundland, Canada. May 31–June 5, 2015. V011T12A008. ASME. https://doi.org/10.1115/OMAE2015-41725.

Tschoepe, E.C., Wolfe, G.K., 1981. SPM hose test program. In: Offshore Technology Conference Proceeding - OTC 4015. May 4–7, 1981. OnePetro, Houston, Texas, USA, pp. 71–80. https://doi.org/10.4043/4015-MS.

Venugopal, V., Varyani, K.S., Barltrop, N.D.P., 2006. Wave force coefficients for horizontally submerged rectangular cylinders. Ocean Eng. 33 (11–12), 1669–1704. https://doi.org/10.1016/j.oceaneng.2005.09.007.

Venugopal, V., Varyani, K.S., Westlake, P.C., 2009. Drag and inertia coefficients for horizontally submerged rectangular cylinders in waves and currents. Proc. IME M J. Eng. Marit. Environ. 223 (1), 121–136. https://doi.org/10.1243/14750902JEME124, 2009.

Vugts, Jan H., 1968. The hydrodynamic coefficients for swaying, heaving and rolling cylinders in a free surface, 1968. Report number 194-P/TNO Report No. 112 S, TUDelft, Faculty of Marine Technology, Ship Hydromechanics Laboratory Report 194-P, Nederlands Scheepsstudiecentrum TNO, Shipbuilding Department, Delft, The Netherlands Int. Shipbuid. Prog. 15 (167), 251–276. https://doi.org/10.3233/ISP-1968-1516702. Available at: http://resolver.tudelft.nl/uuid:5c647df4-3f70-4451-8895-13d1f08bf769. (Accessed 11 September 2021).

Wang, D., Sun, S., 2014. An analytical solution of wave exciting loads on CALM buoy with skirt. Appl. Mech. Mater. 478, 254–258. https://doi.org/10.4028/www.scientific.net/AMM.477-478.254.

Wang, D., Sun, S., 2015. Study of the radiation problem for a CALM buoy with skirt. Ship Build. China 56 (1), 95–101.

Wang, F., Chen, J., Gao, S., Tang, K., Meng, X., 2017a. Development and sea trial of real-time offshore pipeline installation monitoring system. Ocean Eng. 146, 468–476. https://doi.org/10.1016/j.oceaneng.2017.09.016.

Wang, H., Ma, G., Sun, L., Hu, K., 2017b. Model test and coupled dynamic analysis of a deepwater FPSO with internal turret mooring system. Brodogradnja 68 (4), 42–55. https://doi.org/10.21278/brod68403.

Wichers, J., 2013. Guide to Single Point Moorings. Wichers Inc. & CreateSpace Independent Publishing. Available at: http://www.wmooring.com/files/Guide_to_Single_Point_Moorings.pdf. (Accessed 11 September 2021).

Wilson, J.F., 2003. Dynamics of Offshore Structures, second ed. John Wiley and Sons, New Jersey, USA.

Woodburn, P., Gallagher, P., Naciri, M., Borleteau, J., 2005. Coupled CFD simulation of the response of a CALM buoy in waves. In: Proceedings of the ASME 2005 24th International Conference on Offshore Mechanics and Arctic Engineering. 24th International Conference on Offshore Mechanics and Arctic Engineering: Volume 3. Halkidiki, Greece. June 12–17, 2005. ASME, pp. 793–803. https://doi.org/10.1115/OMAE2005-67063.

Ye, J., 1988. A new approach for the bending problem of shallow shell by the boundary element method. Appl. Math. Model. 12 (5), 467–470. https://doi.org/10.1016/0307-904x(88)90083-2.

Young, R.A., Brogren, E.E., Chakrabarti, S.K., 1980. Behavior of loading hose models in laboratory waves and currents. In: Offshore Technology Conference Proceeding, OTC-3842-MS. Houston, Texas, USA, pp. 421–428. https://doi.org/10.4043/3842-MS.

Zhang, S., Chen, C., Zhang, Q.-X., Zhang, D.-M., Zhang, F., 2015. Wave loads computation for offshore floating hose based on partially immersed cylinder model of improved Morison formula. Open Petrol. Eng. J. 8, 130–137. https://doi.org/10.2174/1874834101508010130.

Ziccardi, J.J., Robins, H.J., 1970. Selection of the hose systems for SPM tanker terminals. In: OTC 1152, 2nd Annual Offshore Technology Conference, Houston, 1970 Paper Presented at the Offshore Technology Conference, Houston, Texas, April 1970. Paper Number: OTC-1152-MS. https://doi.org/10.4043/1152-MS.

Zou, J., Harrell, R., 2017. New semisubmersible design increases safety, lower costs, improves project delivery time and is riser friendly. White paper, houston offshore new semi design, USA. Available At: https://www.researchgate.net/publication/330259811_Houston_Offshore_New_Semi_Design, 4th December, 2021.

Zou, J., Poll, P., Roddier, D., Tom, N., Peiffer, A., 2013. VIM testing of a paired column semi-submersible. In: Proceedings of International Conference on Ocean, Offshore and Arctic Engineering, June 9-14, 2013, Nantes, France. OMAE2013-10001, vol. 7. https://doi.org/10.1115/OMAE2013-10001. CFD and vol. IV.

Zou, J., Poll, P., Antony, A., Das, S., Padmanabhan, R., Vinayan, V., Parambath, A., 2014. VIM model testing and VIM induced mooring fatigue of a dry tree paired-column semisubmersible platform. Offshore Technol. Confer. https://doi.org/10.4043/25427-MS.

Yokohama (2016). Seaflex Yokohama Offshore Loading & Discharge Hose. The Yokohama Rubber Co. Ltd. Hiratsuka City, Japan. Available at: https://www.y-yokohama.com/global/product/mb/pdf/resource/seaflex.pdf Accessed on 17th May 2021.

Trelleborg (2017). Surface Buoyancy. Trelleborg Marine and Infrastructure. Product Brochure, Report Number BC-SUR v1.3-EN. Trelleborg, Sweden. Available at: https://www.trelleborg.com/en/marine-and-infrastructure/products-solutions-and-services/marine/surface-buoyancy. Accessed on 17th November, 2021.

Esmailzadeh, E, Goodarzi, A., 2001b. Robust stability and dynamic analysis of a special type of floating offshore structure. In: Proceedings of the ASME 2001 International Mechanical Engineering Congress and Exposition. Vibration and Control of Mechanical Systems. New York, New York, USA. November 11–16, 2001. ASME, pp. 211–216. https://doi.org/10.1115/IMECE2001/DE-23227.

Lee, D.H., Choi, H.S. (2002). A nonlinear stability analysis of tandem offloading systems. 24th Symposium on Naval Hydrodynamics, Fukuoka, Japan, 8-13 July, 2002. Page 348-359. Available at: https://www.nap.edu/read/10834/chapter/25 (Accessed on: 24th December, 2021.).

Lee, D.H., Choi, H.S. (2005). A stability analysis of tandem offloading systems at sea. J. Mar. Sci. Technol. 10, 53–60 (2005). https://doi.org/10.1007/s00773-005-0196-z.

Sphaier, S.H., Fernandes, A.C., Correa, S.H.S., and Castro, G.A.V. (2002). Maneuvering model for FPSOs and stability analysis of the offloading operation, ASME. J. Offshore Mech. Arct. Eng. November 2002; 124(4): 196–202. https://doi.org/10.1115/1.1513175.